Introduction to Soft X-ray Laser and Its Application

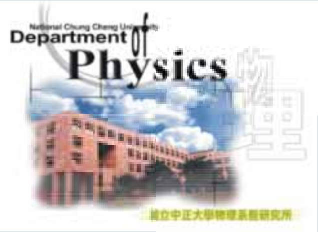

J.Y. Lin[1](林俊元), S.Y. Chen[2,3], H.H. Chu[3], & J. Wang[2,3]

[1] Department of Physics, CCU, Taiwan
[2] IAMS, Academia Sinica, Taiwan
[3] Department of Physics, NCU, Taiwan

Outline

I. Next generation x-ray source

II. 10 TW & 100 TW femtosecond laser system

III. Generations of collisional excitation OFI X-ray lasers in a clustered gas jet

V. Applications with soft X-ray lasers

How can we generate X-rays?

Coolidge Tube

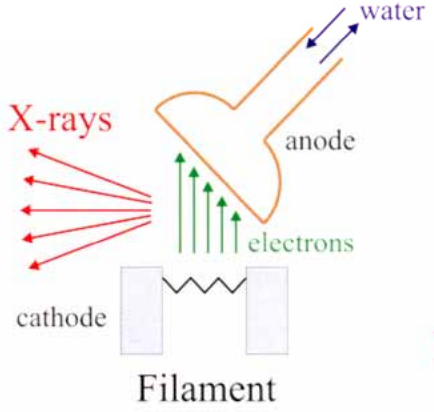

Rotating Anode

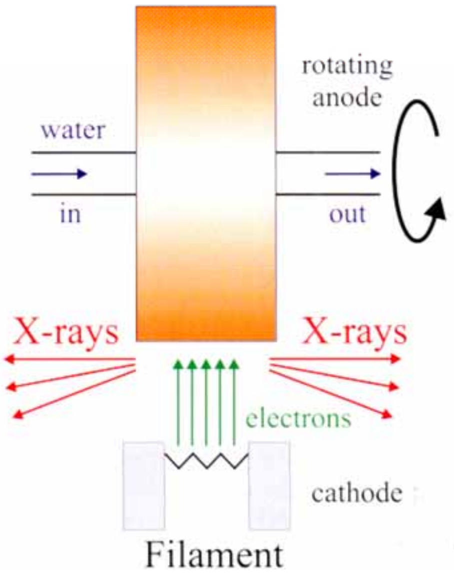

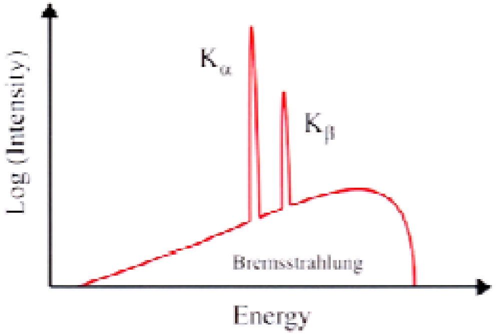

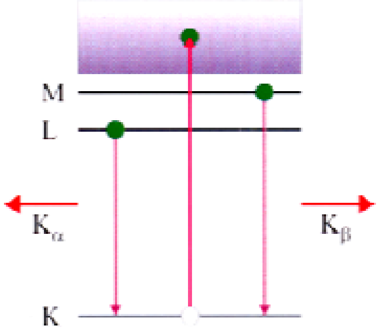

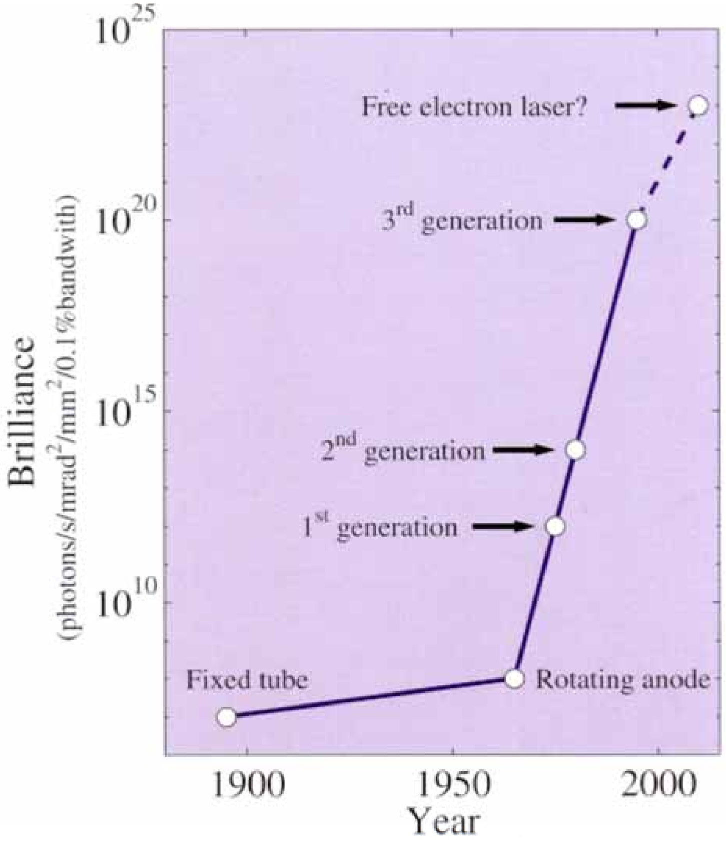

Next / New generation x-ray sources

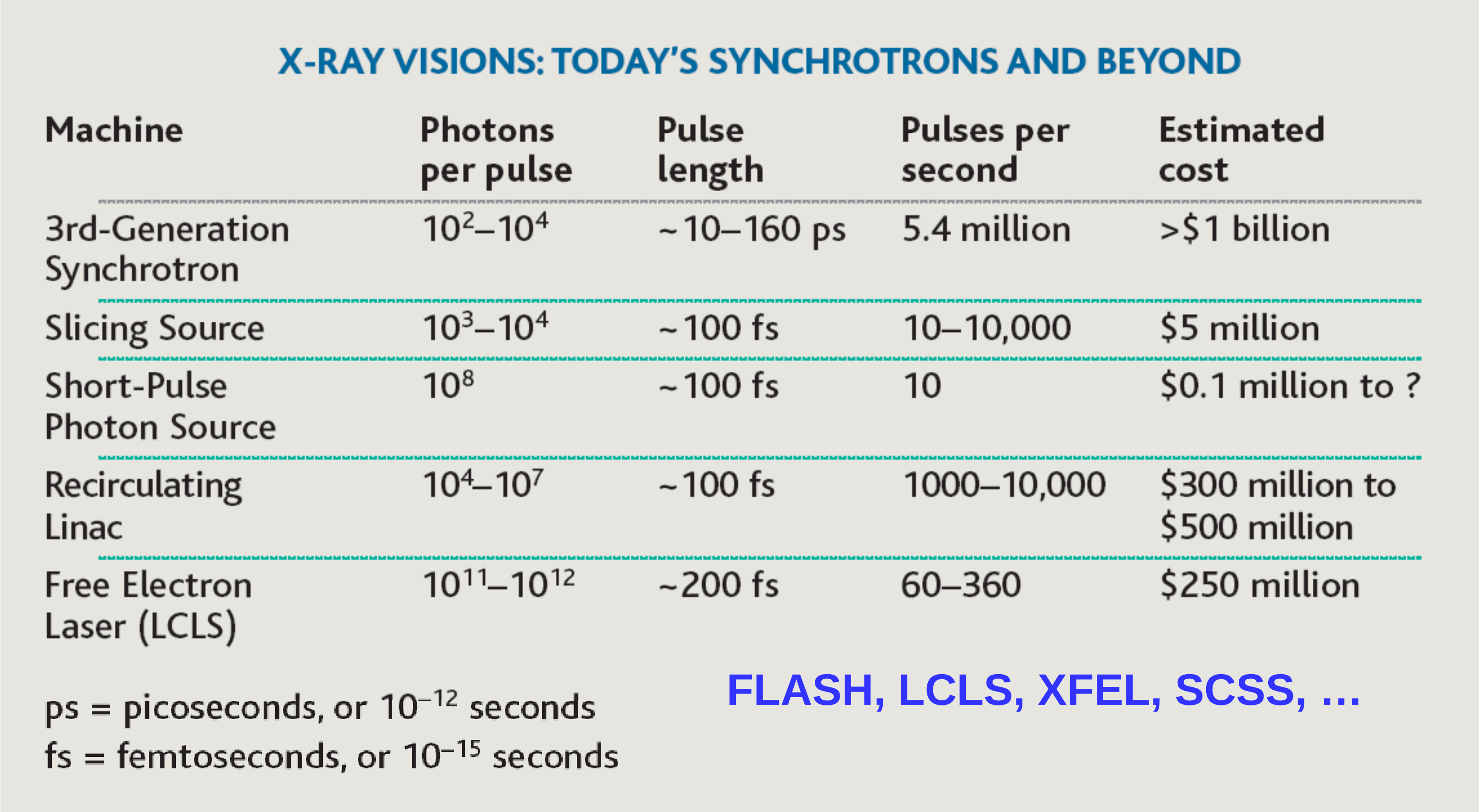

X-RAY VISIONS: TODAY'S SYNCHROTRONS AND BEYOND

Machine	**Photons per pulse**	**Pulse length**	**Pulses per second**	**Estimated cost**
3rd-Generation Synchrotron	10^2–10^4	~10–160 ps	5.4 million	>$1 billion
Slicing Source	10^3–10^4	~100 fs	10–10,000	$5 million
Short-Pulse Photon Source	10^8	~100 fs	10	$0.1 million to ?
Recirculating Linac	10^4–10^7	~100 fs	1000–10,000	$300 million to $500 million
Free Electron Laser (LCLS)	10^{11}–10^{12}	~200 fs	60–360	$250 million

ps = picoseconds, or 10^{-12} seconds

fs = femtoseconds, or 10^{-15} seconds

FLASH, LCLS, XFEL, SCSS, …

High-Power Short-Pulse X-ray Lasers -- black horse technology

Science **298**, 1356 (2002)

註：short-pulse photon source 是計劃附加於美國Stanford 直線加速器之儀器，因此所需經費較低。

Motivation for the development of tabletop soft x-ray lasers?

- Fulfill our scientific curiosity

  →New physics in light-matter interaction

  →Push laser actions toward shorter wavelengths

- Provide compact, coherent, high brightness, high temporal resolution short wavelength light source for applications

  → X-ray Lithography, Microscopy, Tomography… etc

Characteristics of soft x-ray / EUV lasers

- Lasing Wavelength: few to 10’s nm
- Gain Medium: Highly ionized plasma with closed shell configuration
- Pumping Source: High power/energy laser & high voltage discharge
- Operation Mode: Single pass or half cavity gain length product GL > 5

Simplified 3-level laser

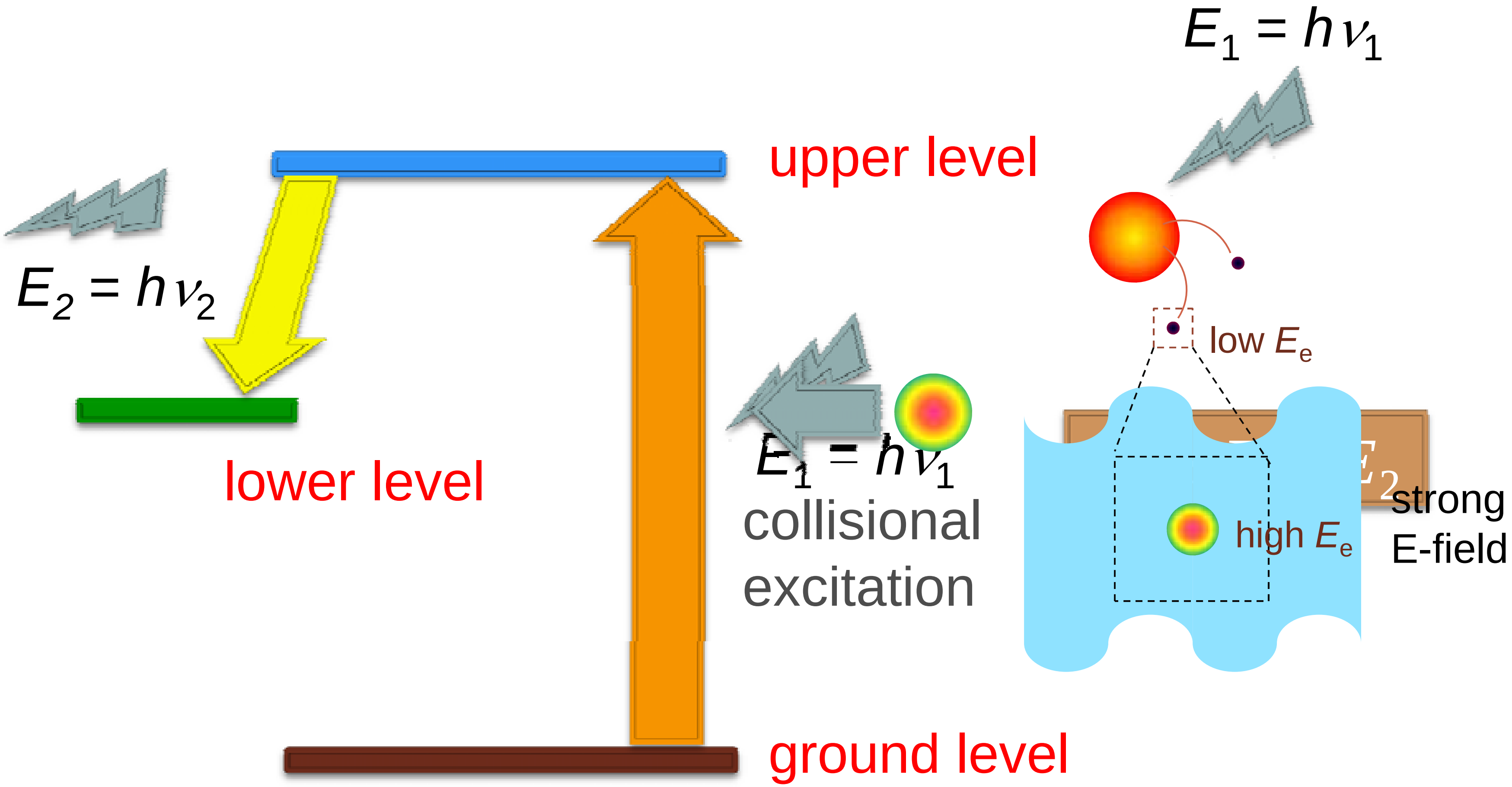

$E_1 = h\nu_1$

upper level

$E_2 = h\nu_2$

lower level

$E_1 = h\nu_1$

collisional excitation

low E_e

E_2

strong E-field

high E_e

ground level

$E_e > \sim \Delta E > E1 > E_2$

Energy diagram of collisional excitation soft x-ray laser in Ne-like Ar ions

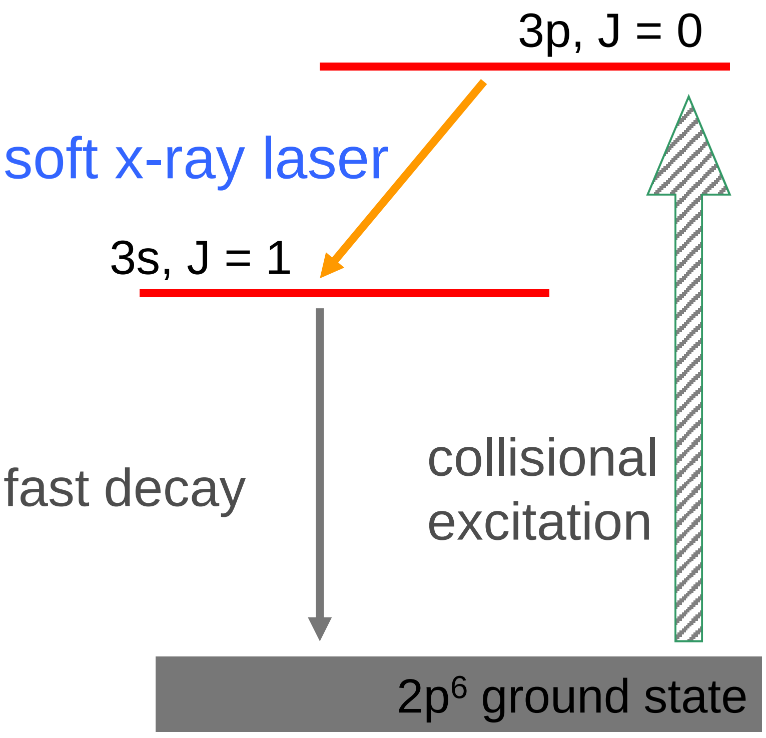

3p, J = 0

soft x-ray laser

3s, J = 1

fast decay

collisional excitation

$2p^6$ ground state

Ne-like Ar

Relative Ion Abundance

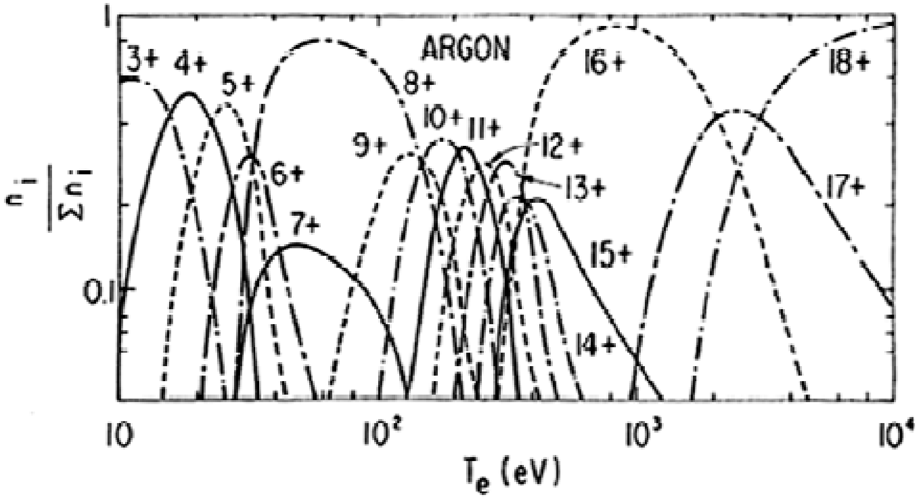

Origin of x-ray laser: Star War

Jeff Hecht

The History of the X-ray Laser

The long and curious history of the X-ray laser began in an effort to expand the frontier of knowledge and culminated in one of the wildest schemes ever pursued by the United States government—the "Star Wars" missile defense initiative in the 1980s. Today, the X-ray laser is finally realizing its initial potential as a research tool for studying molecular-scale structures.

This artist's concept shows beams from three X-ray rods destroying Cold War targets after detonation of the bomb powering the X-ray rods. If deployed in space, each of the thin rods of the X-ray laser weapon would be aimed at an enemy missile.

From Joseph Nilsen, "Legacy of the X-ray Laser Program," Lawrence Livermore National Laboratory report.

First laboratory x-ray laser at 20.6 & 20.9 nm

In 1984

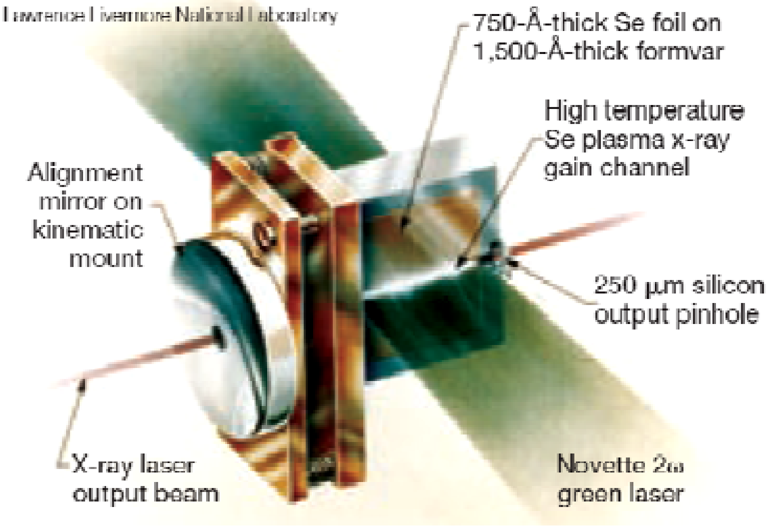

Light from the two Novette arms was focused onto opposite sides of a selenium foil target in Livermore's X-ray laser.

Soft x-ray laser generation

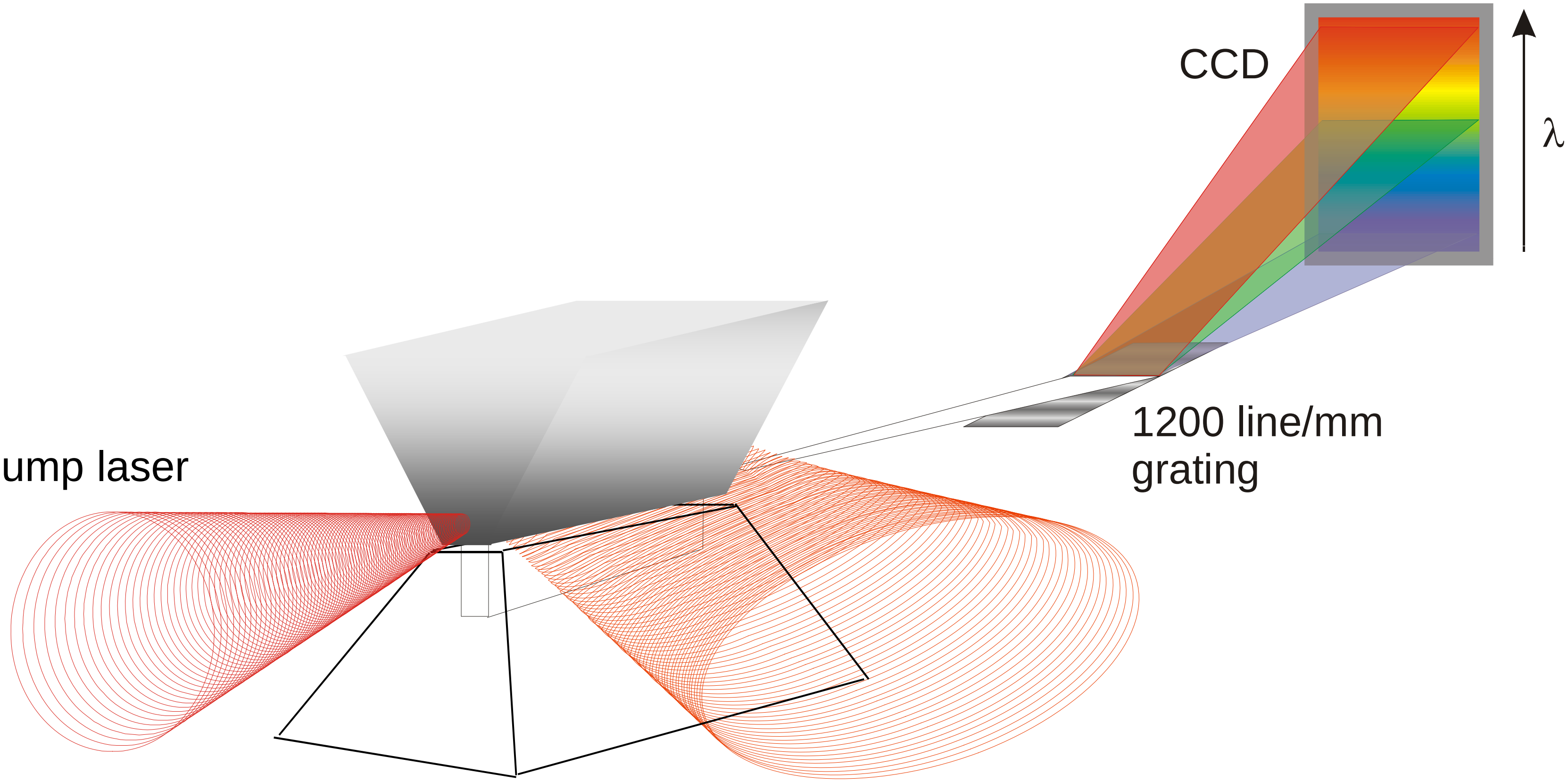

infrared pump laser pulse
beam dia. = few to 10's cm

Ultra-high Power Laser System

Chirped pulse amplification scheme

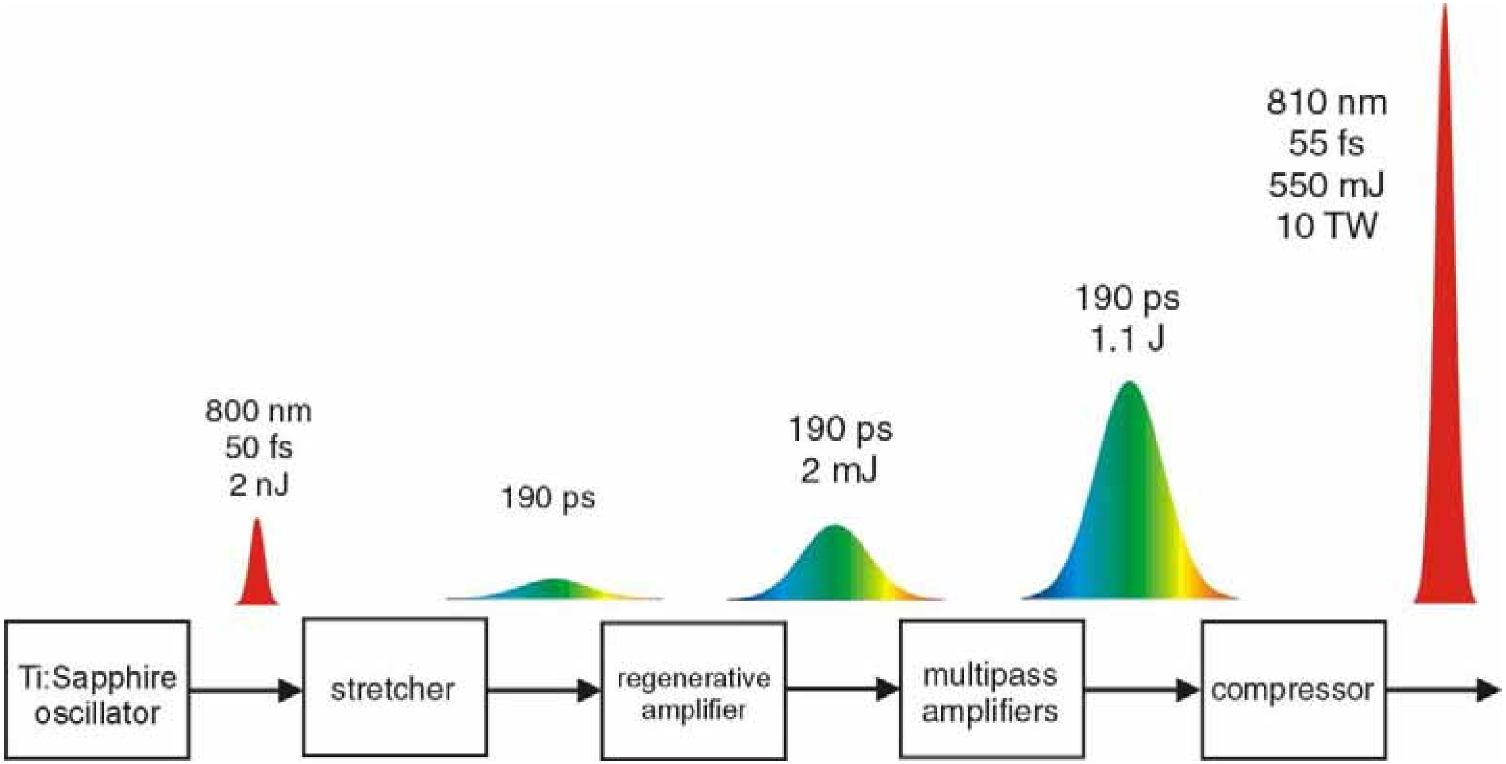

10 TW femtosecond laser system layout

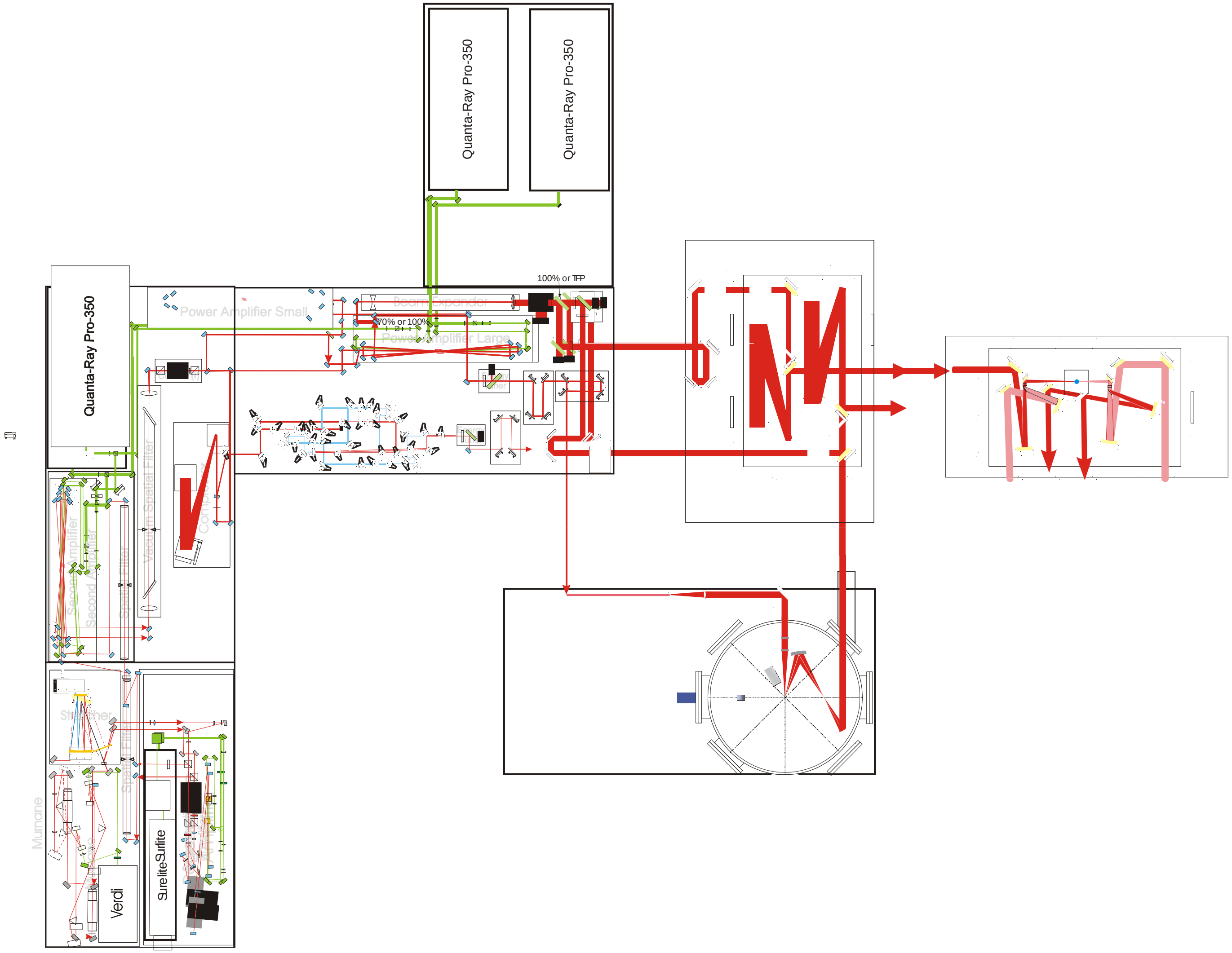

10 TW femtosecond laser system – I

10 TW Laser System

25 fs Oscillator

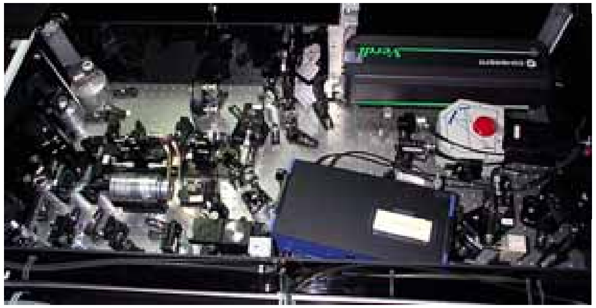

Stretcher

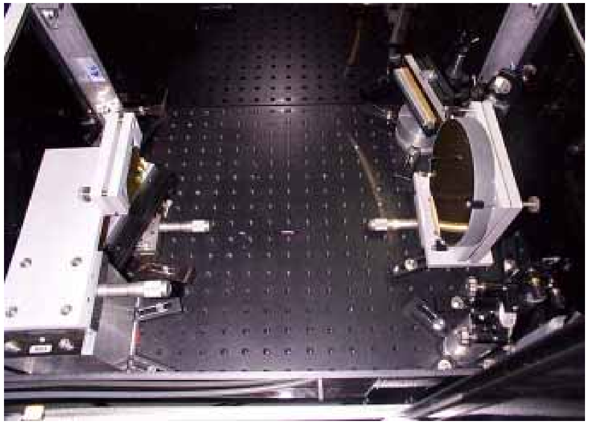

10 TW femtosecond laser system – II

Regenerative Amplifier

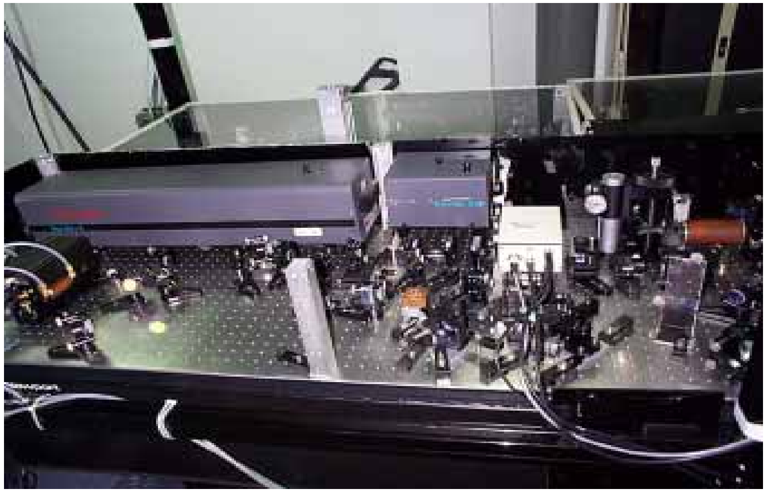

2nd Stage Amplifier

3rd Stage Amplifier

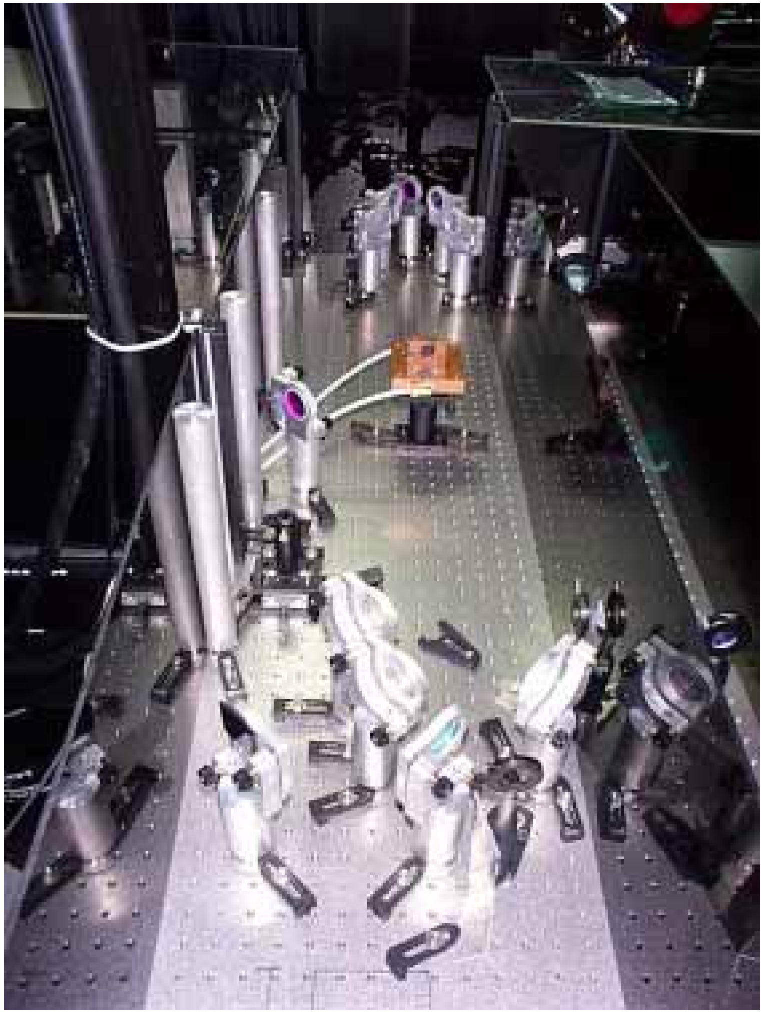

100 TW beamline 5 pass amplifier

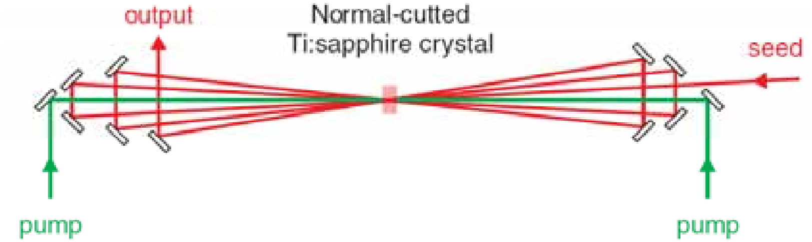

- pump energy = 15.4 J
- output energy = 6.7 J
- operation temperature = -120°C

- cryogenically-cooled crystal mount:

CryoStar, Amplitude Technologies Inc.

100 TW laser system at NCU

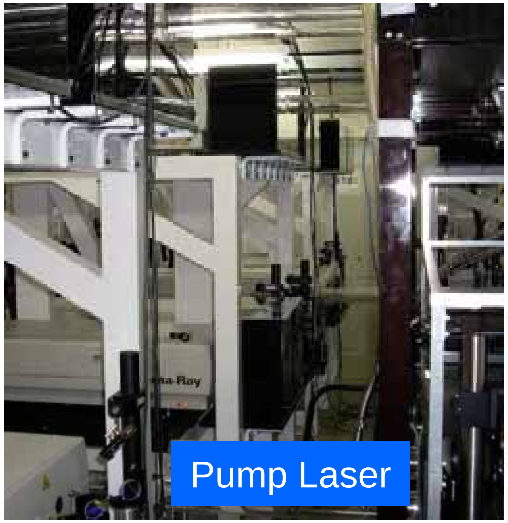

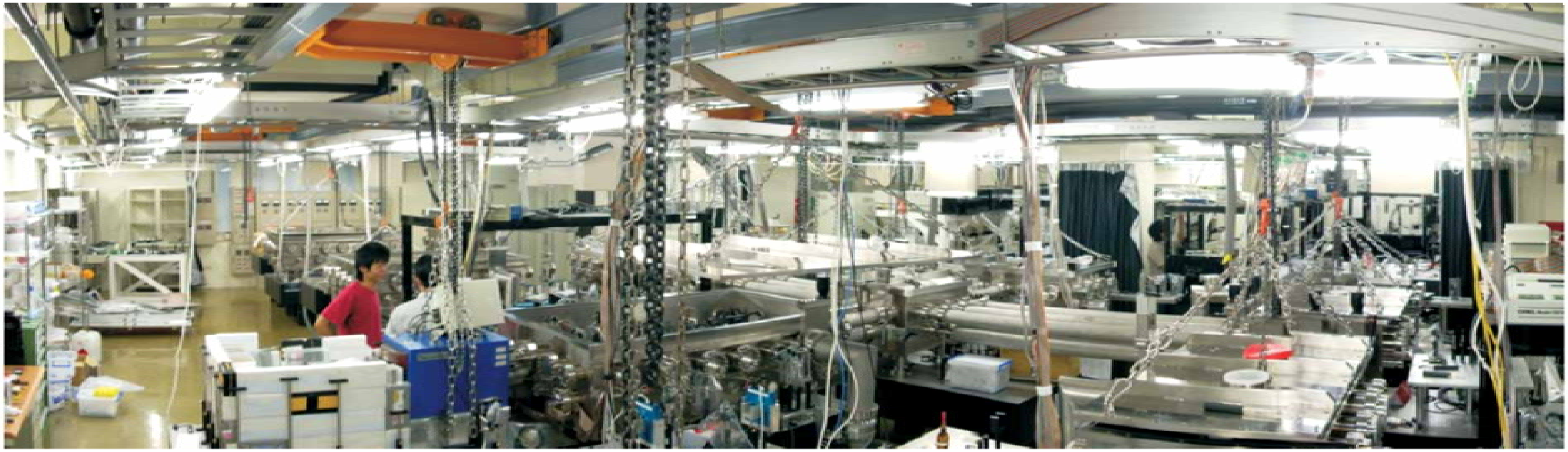

What a100 TW laser pulse can do?

energy $E > 1\ (\mathrm{J})$	Comparison:
focused intensity $I > 10^{20}\ (\mathrm{W/cm^2})$	sun light at noon $I = \ 0.1\ (\mathrm{W/cm^2})$
electric field $\lvert\mathbf{E}_{\mathrm{laser}}\rvert > 10^{11}\ (\mathrm{V/cm})$	hydrogen atom $\lvert\mathbf{E}_H\rvert = 5.1 \times 10^9\ (\mathrm{V/cm})$
magnetic field $\lvert\mathbf{B}_{\mathrm{laser}}\rvert > 9 \times 10^4\ (\mathrm{T})$	superconducting magnetic $\lvert\mathbf{B}_{\mathrm{m}}\rvert \sim 10^2\ (\mathrm{T})$
optical pressure $P_{\mathrm{laser}} > 10^{15}\ (\mathrm{Pa})$	center of the earth $P_{\mathrm{e}} \sim 3.6 \times 10^{11}\ (\mathrm{Pa})$
acceleration of electron $\lvert\mathbf{a}_e\rvert > 10^{23} g$	black hole (mass = m_{Sun}) $\lvert\mathbf{a}_{\mathrm{B}}\rvert \sim 1.6 \times 10^{12} g$

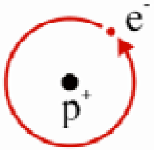

g : gravitational acceleration at the surface of Earth

→ high field science (phenomenal related to high E & B)

The next frontier of Laser Chemistry & Physics

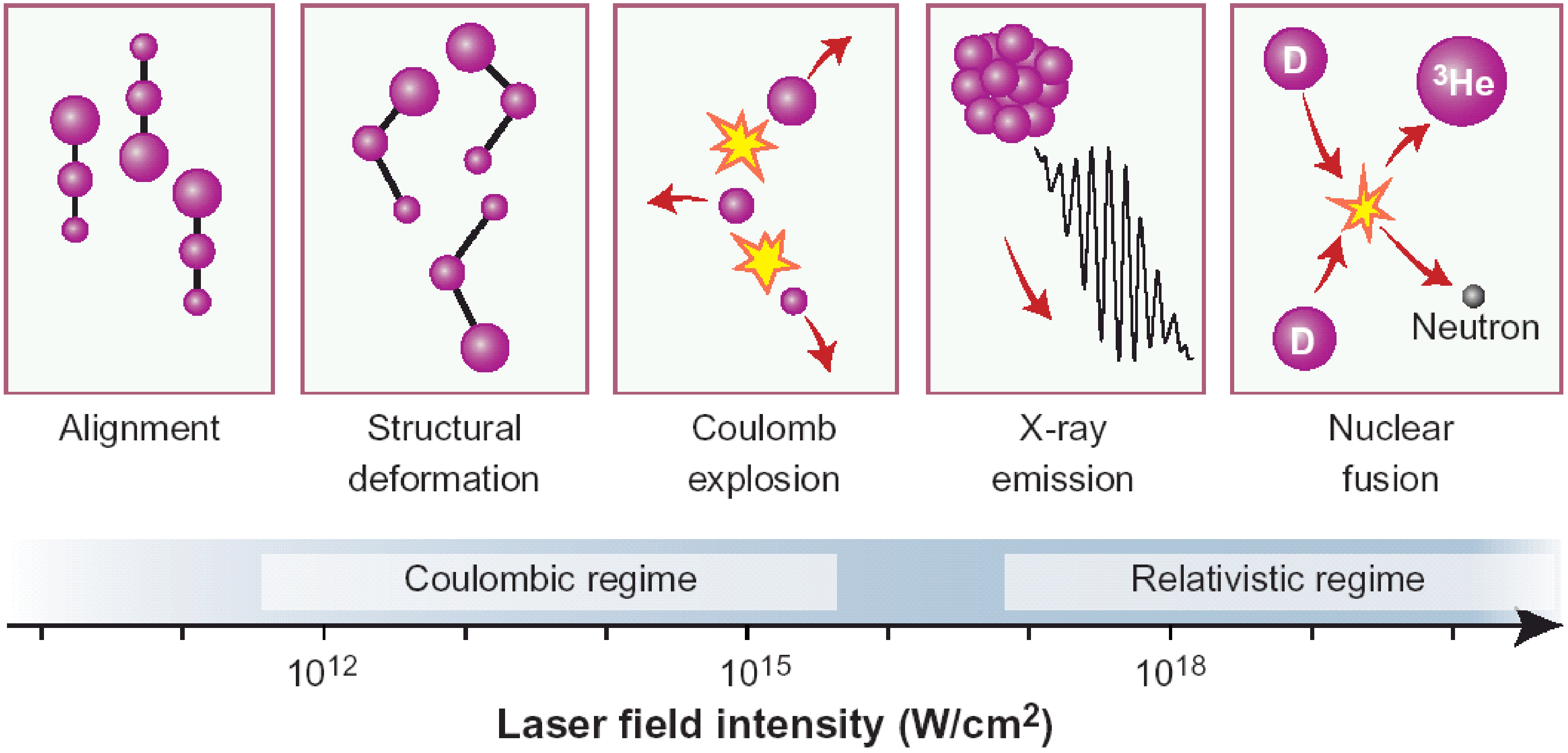

Exotic behavior of molecules and clusters in intense laser fields.

Science **295**, 1659 (2002)

National Ignition Facility

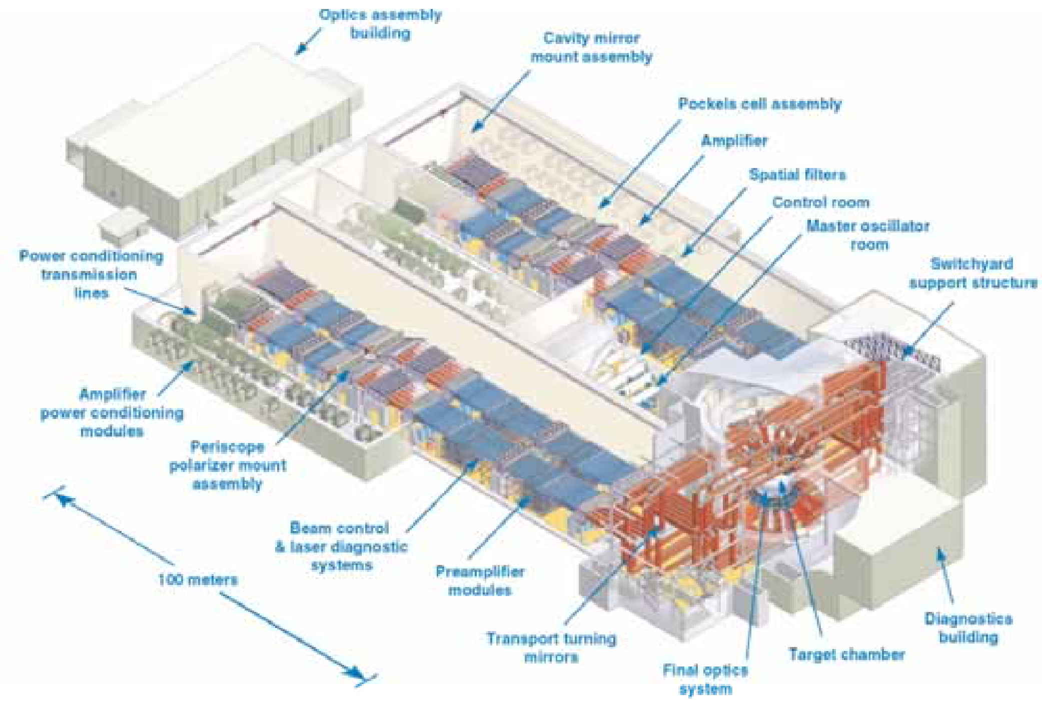

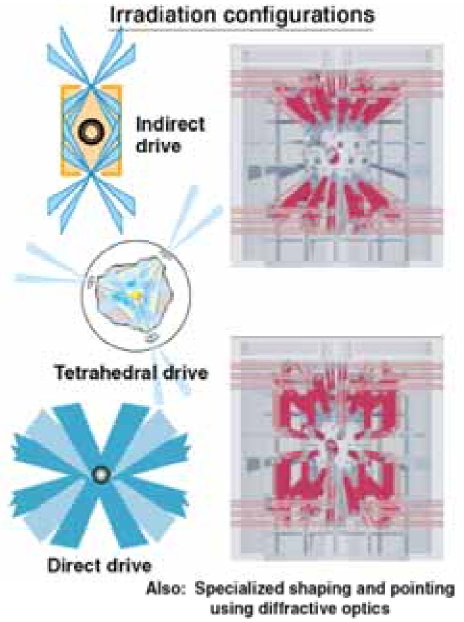

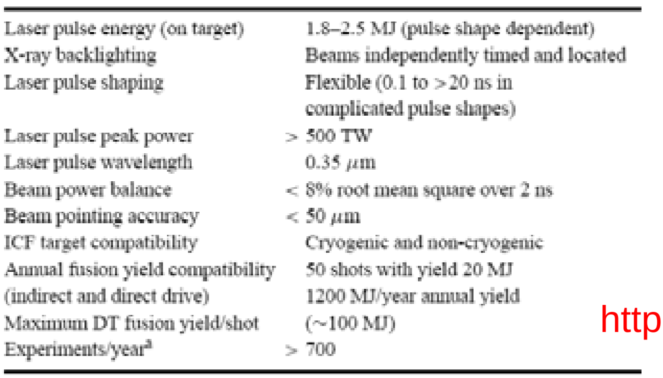

Laser pulse energy (on target)	1.8–2.5 MJ (pulse shape dependent)
X-ray backlighting	Beams independently timed and located
Laser pulse shaping	Flexible (0.1 to >20 ns in complicated pulse shapes)
Laser pulse peak power	> 500 TW
Laser pulse wavelength	0.35 μm
Beam power balance	< 8% root mean square over 2 ns
Beam pointing accuracy	< 50 μm
ICF target compatibility	Cryogenic and non-cryogenic
Annual fusion yield compatibility (indirect and direct drive)	50 shots with yield 20 MJ 1200 MJ/year annual yield
Maximum DT fusion yield/shot	(~100 MJ)
Experiments/year^a	> 700

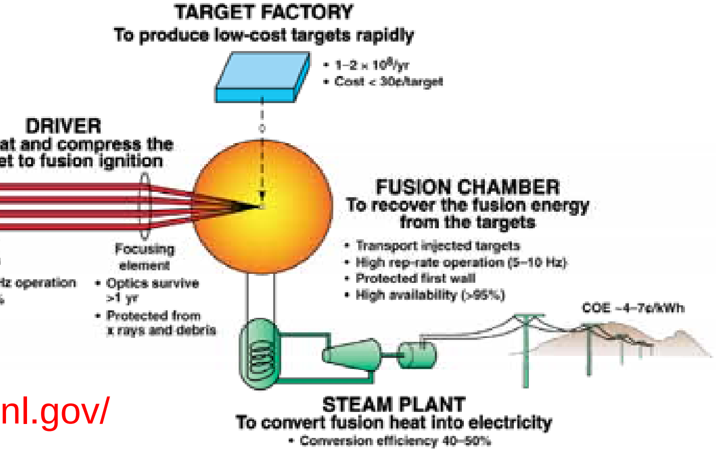

https://lasers.llnl.gov/

Generations of collisional excitation OFI X-ray lasers in a clustered gas jet

Principle of optical-field-ionization x-ray laser

ionization to specific ion stage → heating of electron → electron-ion collisional excitation → population inversion and lasing

↑ tunnelling ionization by strong laser pulse

↑ heating (accelerating) by the laser pulse

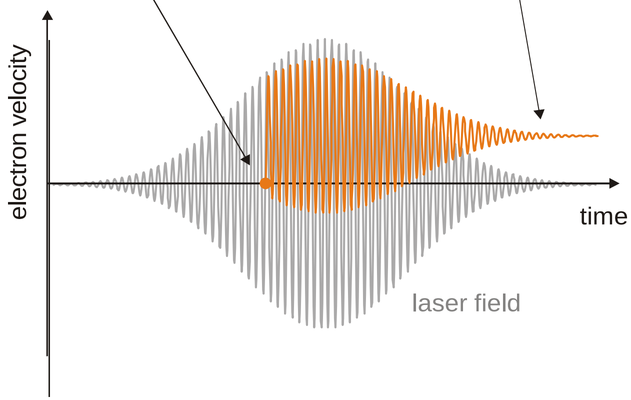

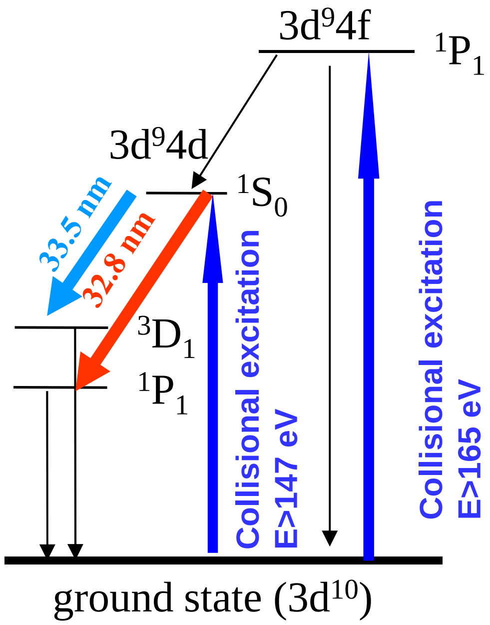

Simplified energy diagram of Ni-like Kr

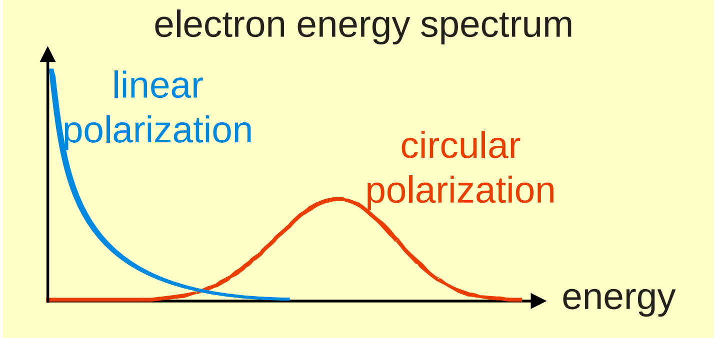

The average electron energy obtained from above-threshold-ionization heating is much higher for a laser pulse of circular polarization than that of linear polarization.

X-ray laser generation with longitudinal pumping

low contamination
@ high repetition rate

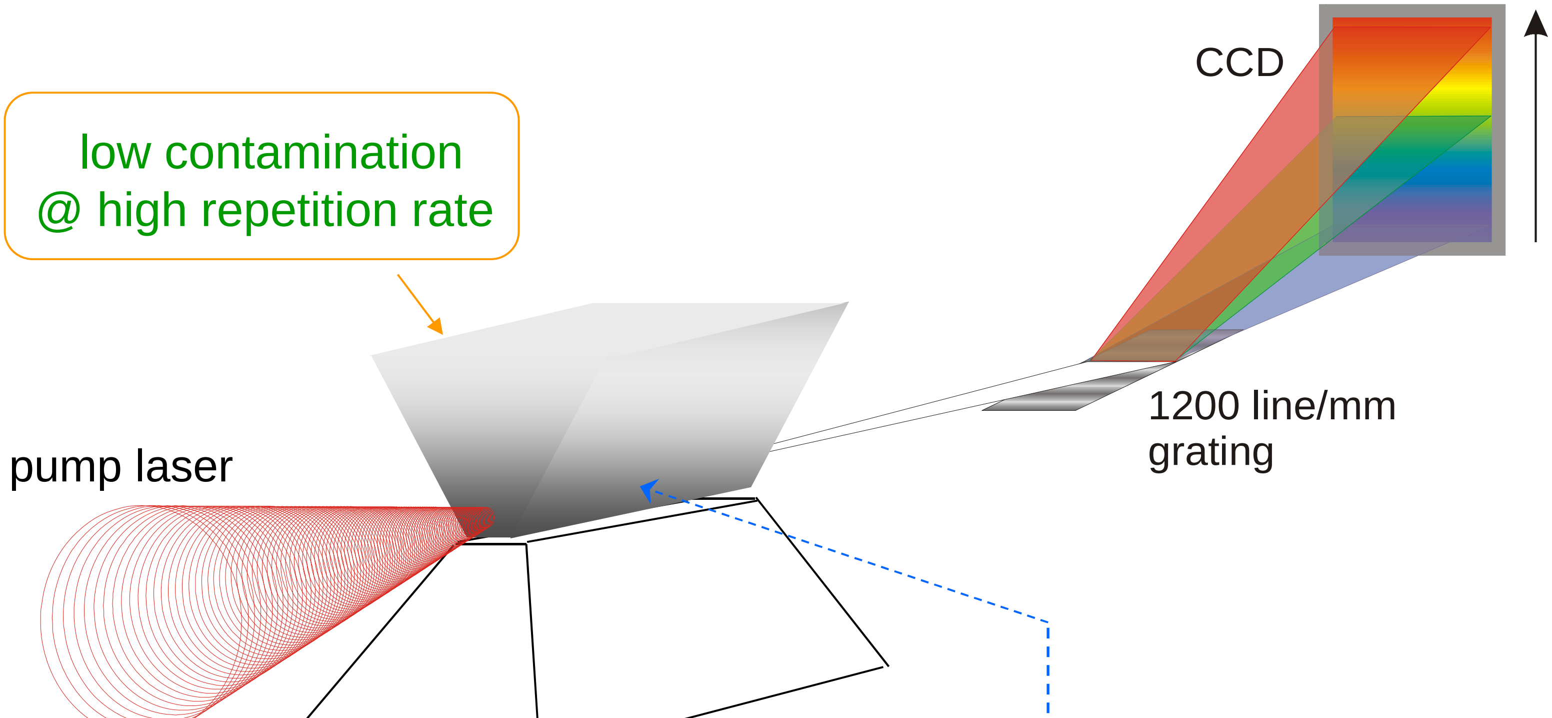

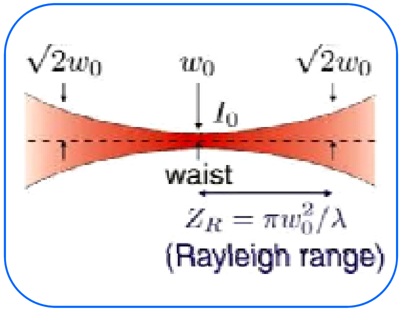

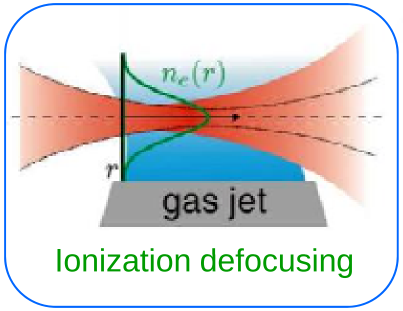

Control of pump laser propagation in plasmas is the key issue for optimizing OFI XRL output !

Diffraction and ionization defocusing effects

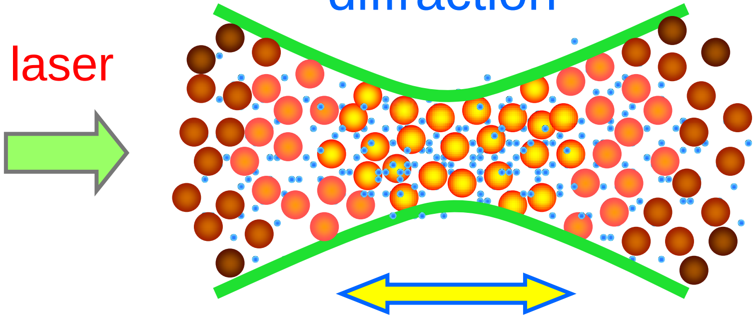

diffraction

laser

gain region

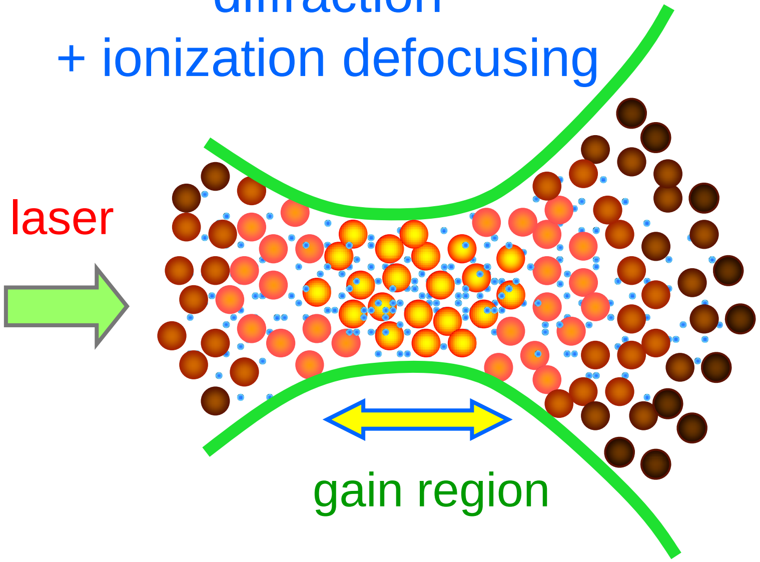

diffraction
+ ionization defocusing

laser

gain region

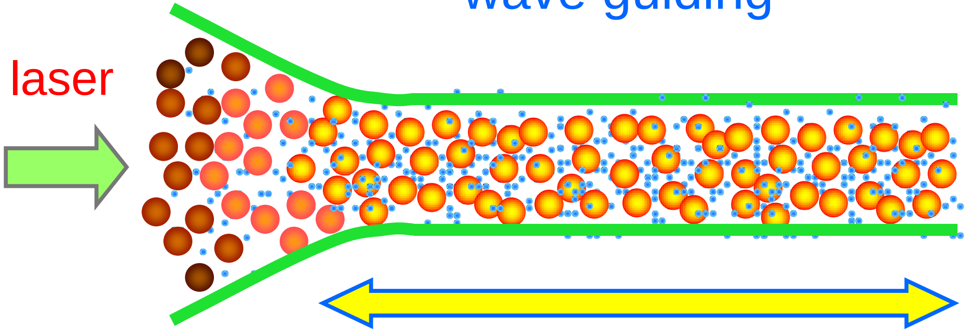

wave guiding

laser

gain region

Efficient guiding of the pump pulse can increase the length of the gain region dramatically !!

Plasma waveguide formation using axicon ignitor-heater scheme

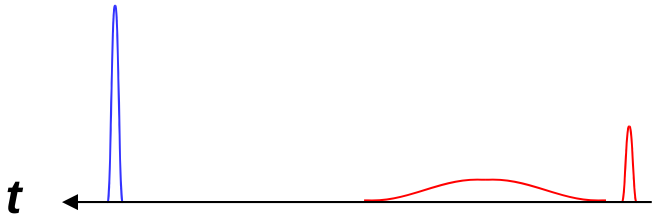

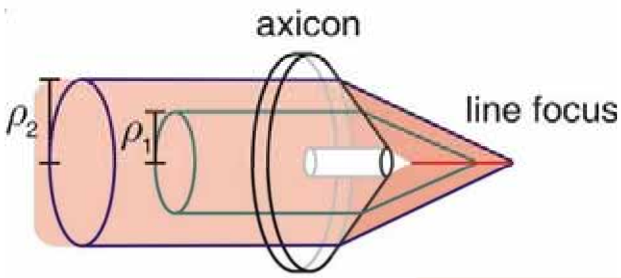

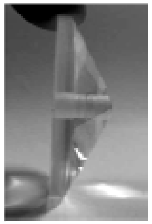

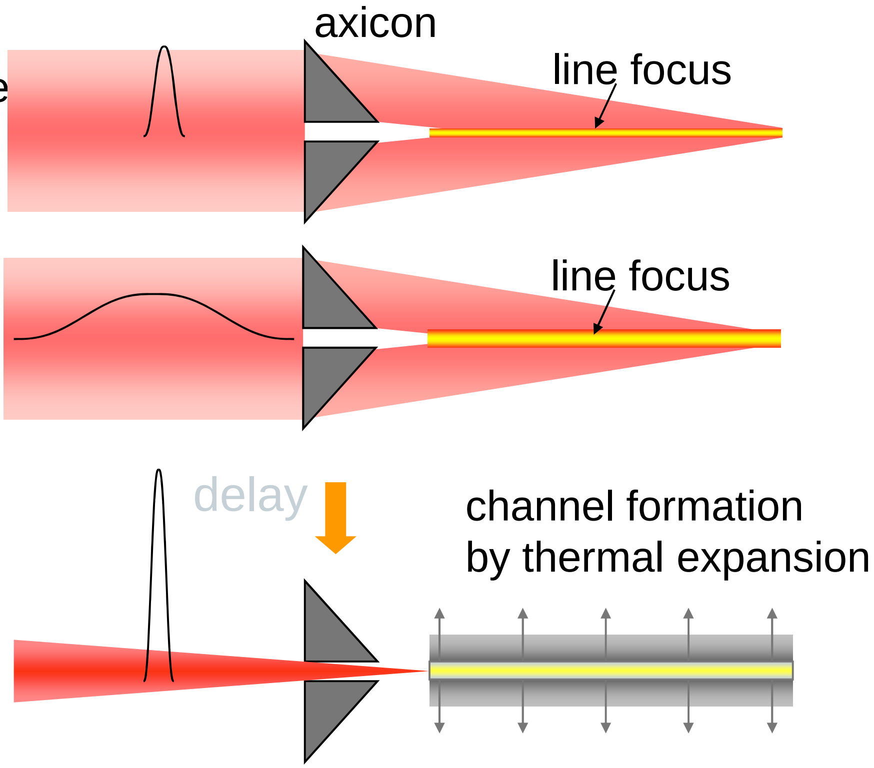

short prepulse
(**Ignitor**)

long prepulse
(**heater**)

pump pulse

axicon

line focus

line focus

delay

channel formation
by thermal expansion

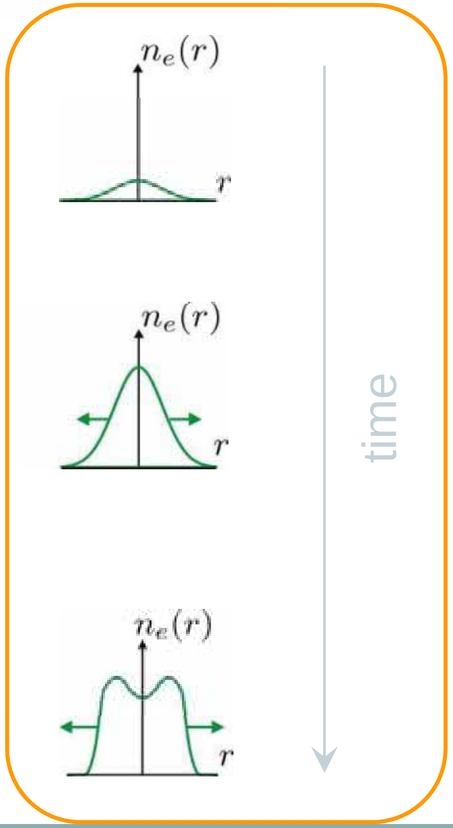

Experimental setup

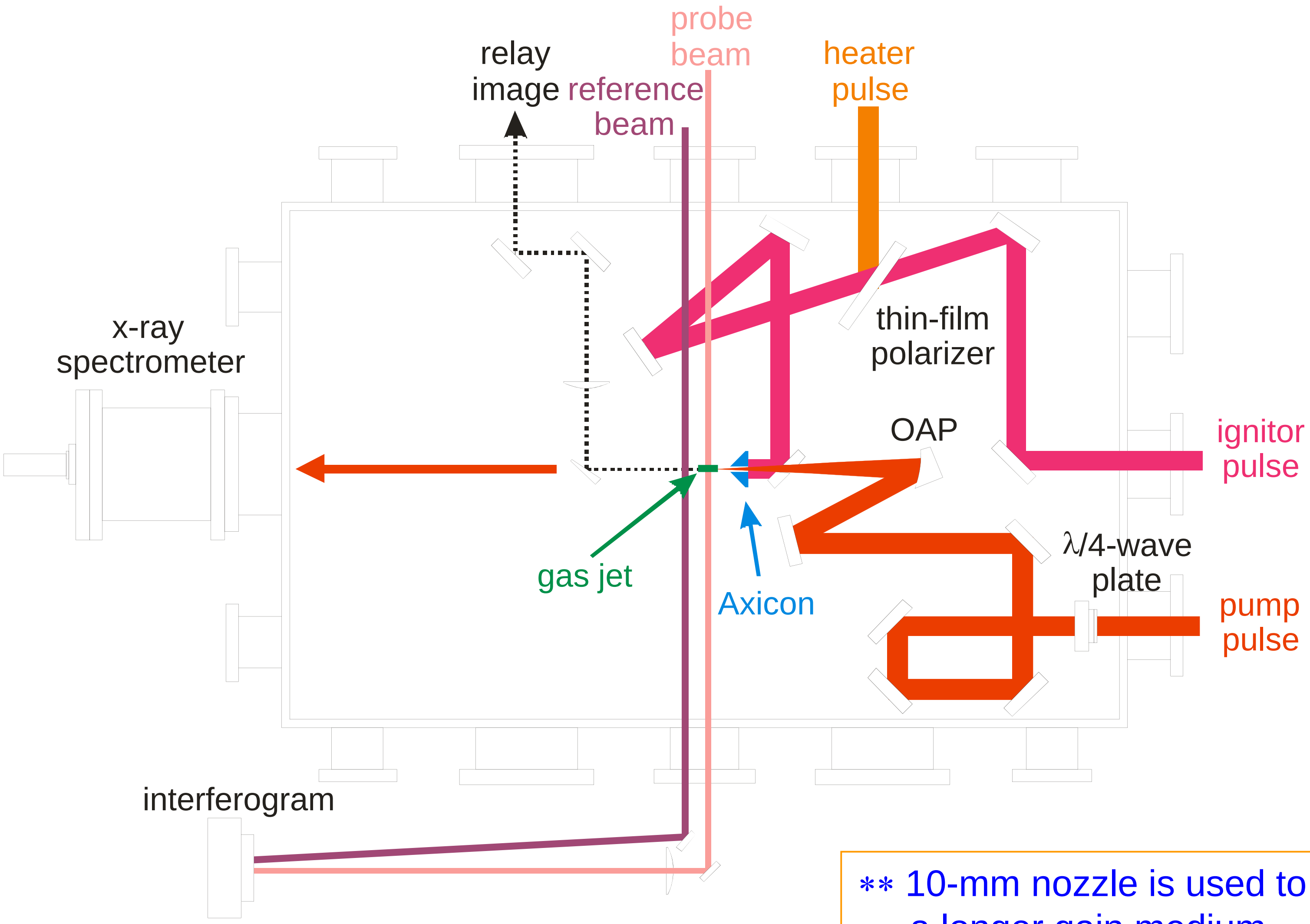

** 10-mm nozzle is used to provide
a longer gain medium

Photography of experimental setup

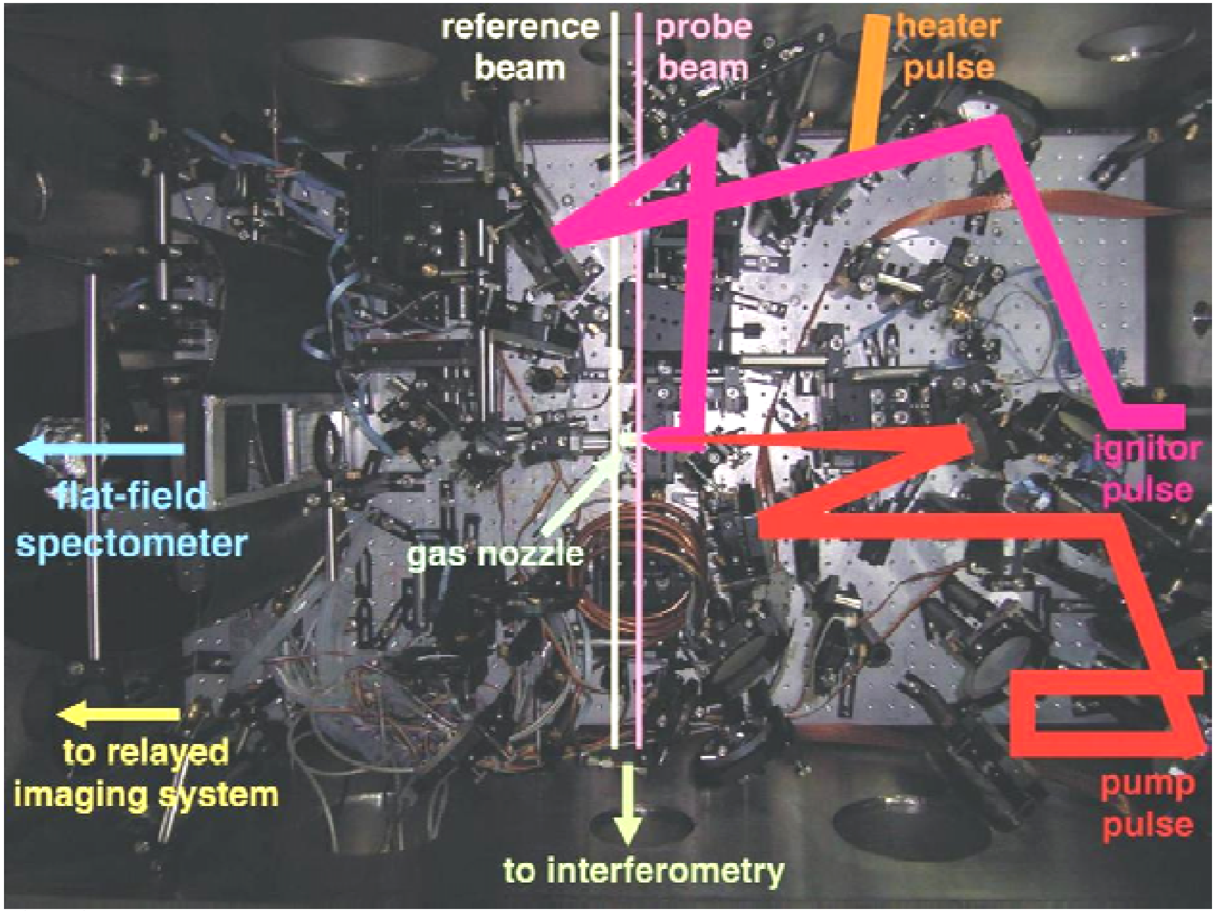

10 cm

Kr lasing at 32.8 nm with & without waveguide

Interferograms in 9-mm gas

(a) without waveguide; N_{atom}: 8×10^{17} cm^{-3}

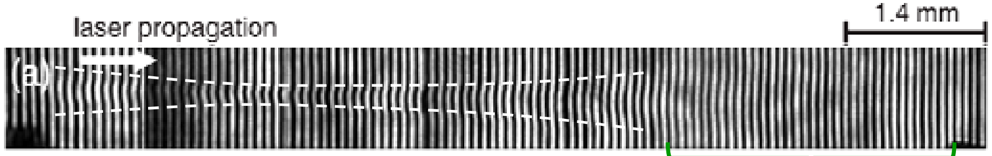

output : 2×10^{8} photons

absorption

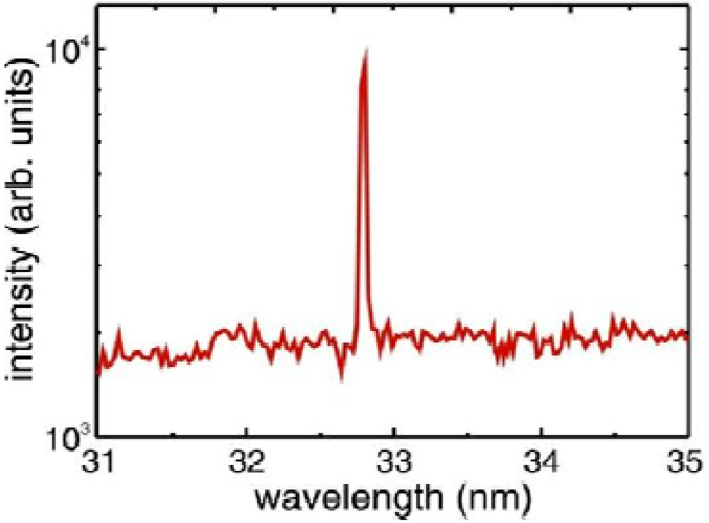

(b) without waveguide; N_{atom}: 1.6×10^{19} cm^{-3}

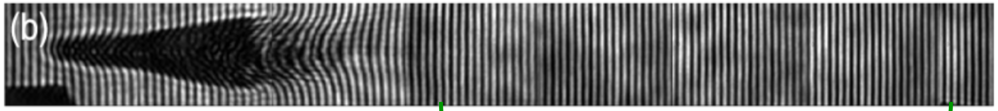

~~output : not detectable~~

absorption

(c) with waveguide; N_{atom}: 1.6×10^{19} cm^{-3}

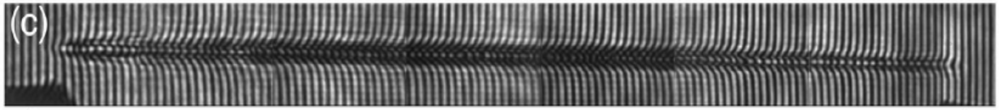

output : $\sim1\times10^{11}$ photons

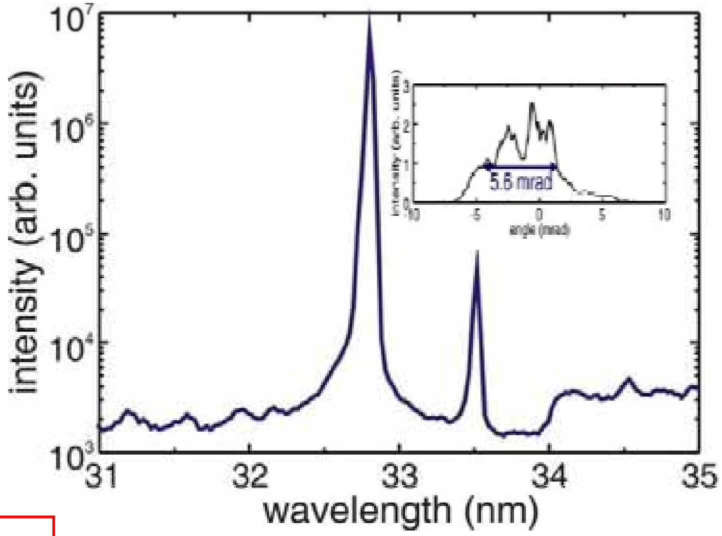

pump pulse: 45 fs, 235 mJ ; focal position: 2750 mm; pump polarization: circular

Dramatic enhancement of OFI X-ray lasing by an optically-preformed plasma waveguide

atom density effect

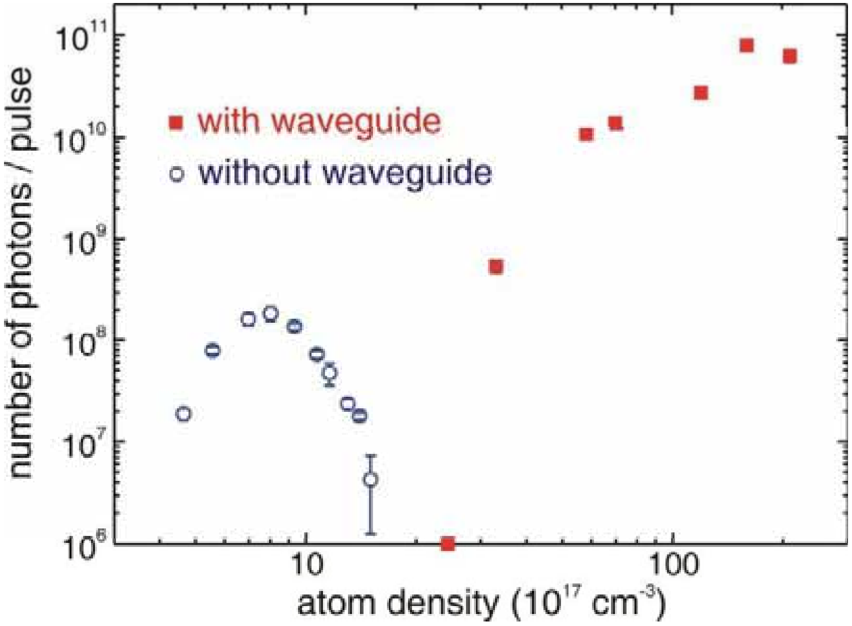

pump energy effect

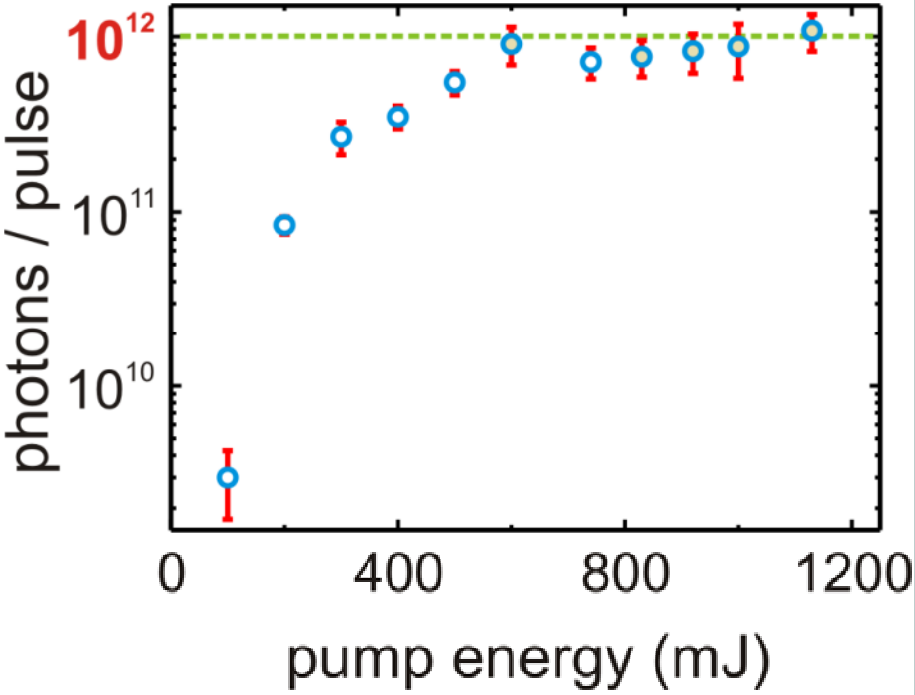

trade-off between larger gain coefficient and more severe ionization defocusing (shorter gain length & longer absorption length)

Soft x-ray lasing spectra and angular distribution in plasma waveguide

Ni-like Kr

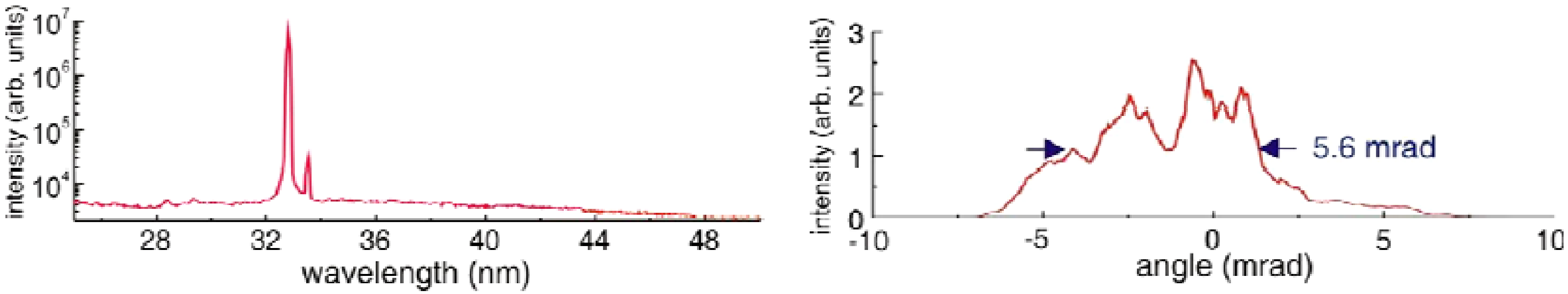

Pd-like Xe

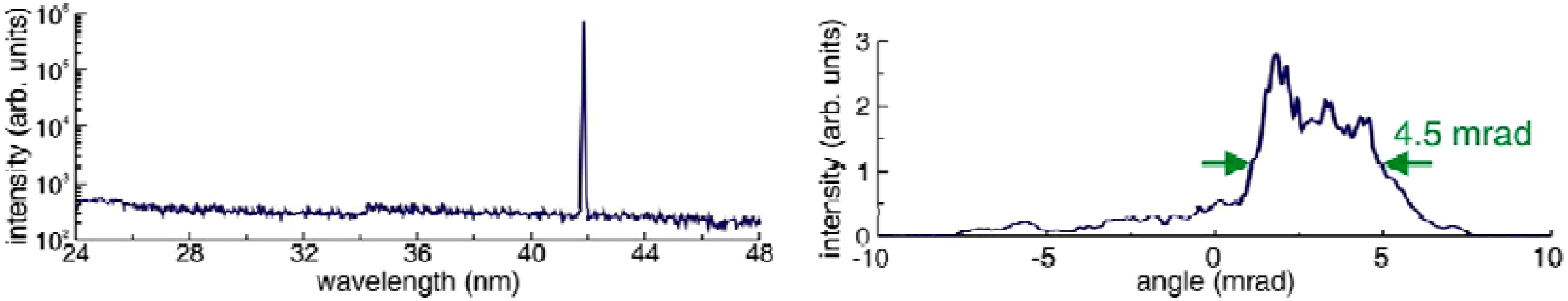

Ne-like Ar

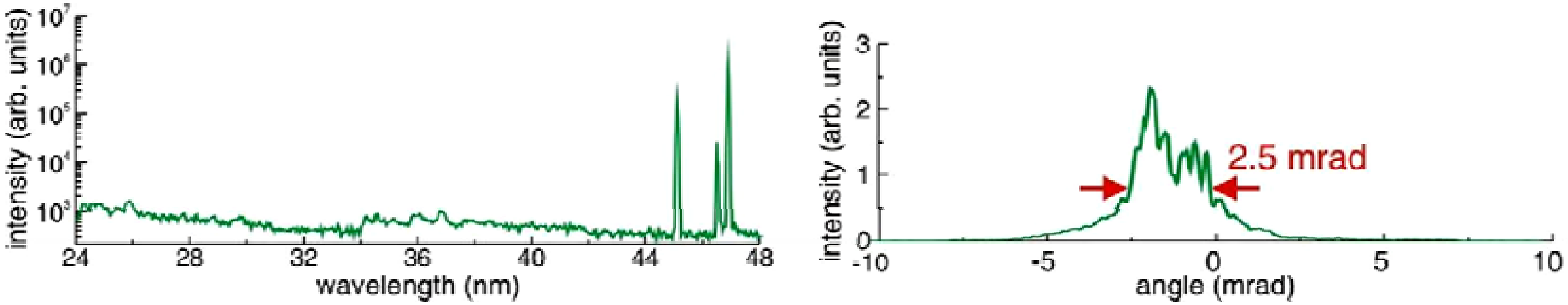

Simultaneous X-ray lasing in two ion species

X-ray spectrum

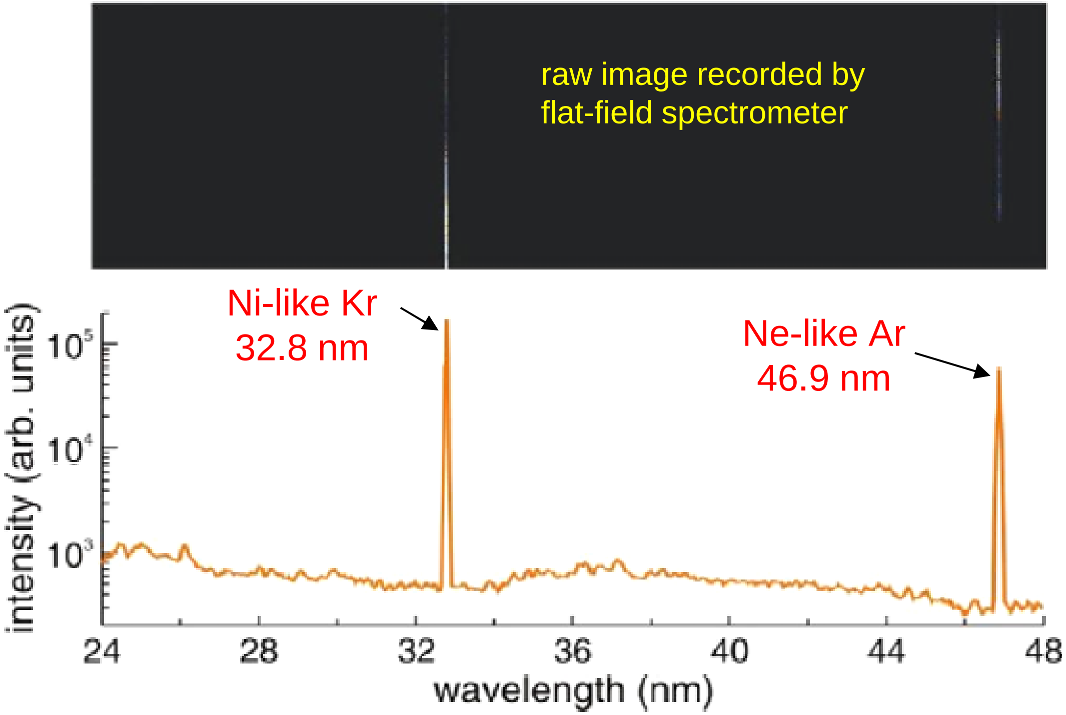

pump pulse: 40 fs, 235 mJ
ignitor: 40 fs, 45 mJ
heater: 160 ps, 260 mJ
Kr atom density: 9.1×10^{18} cm^{-3}
Ar atom density: 1.2×10^{19} cm^{-3}
ignitor-heater separation: 200 ps
hearer-pump delay: 1.5 ns

With a mixed-gas (Kr/Ar~1/1) plasma waveguide x-ray lasing of Ni-like Kr at 32.8 nm and Ne-like Ar at 46.9 nm are obtained simultaneously under adequate conditions.

OFI lasers seeded with HHG in plasma waveguide

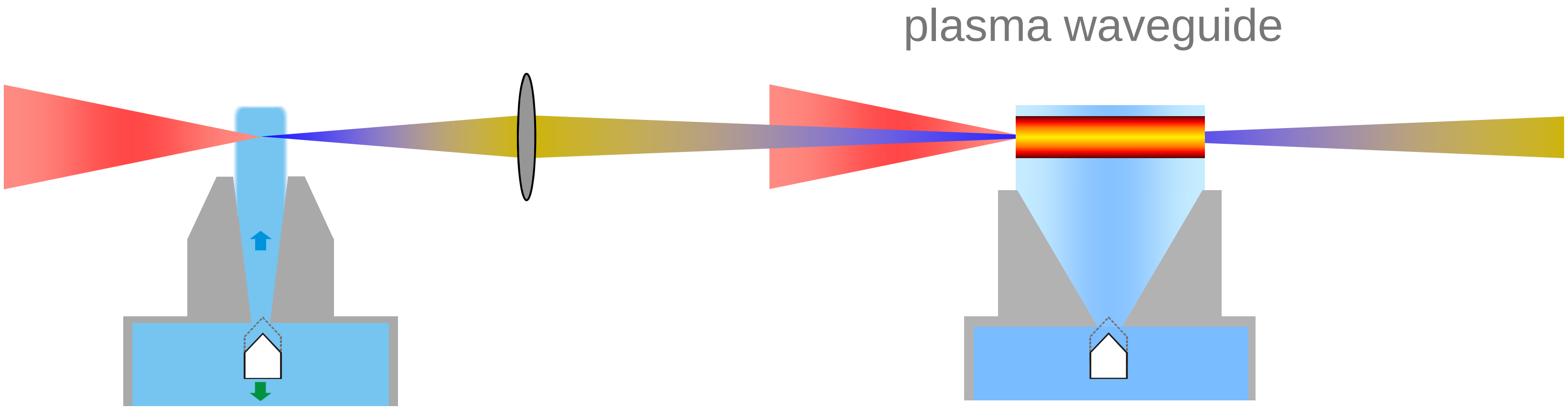

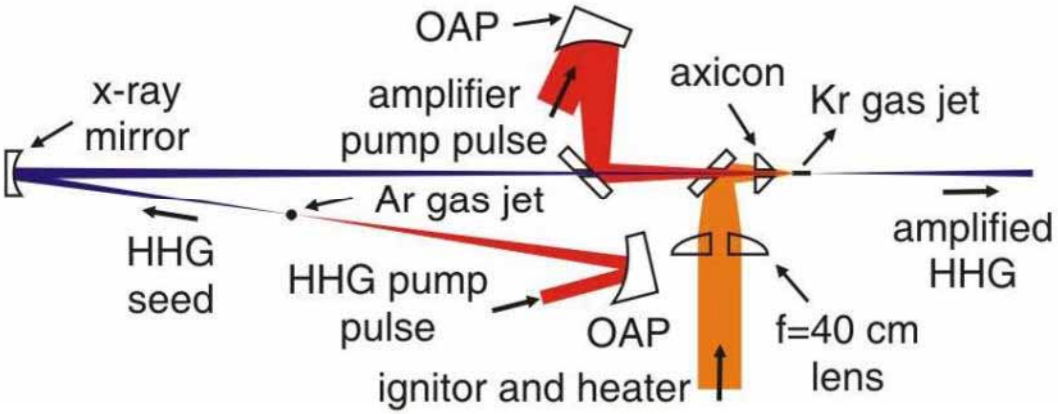

Photon number ↑ (> 10^{11} ?)

Beam divergence ↓ (~ 1 mrad ?)

Pulse duration ↓ (< 1 ps ?)

Polarization state: controllable

OFI X-ray lasers seeded with HHG in plasma waveguide

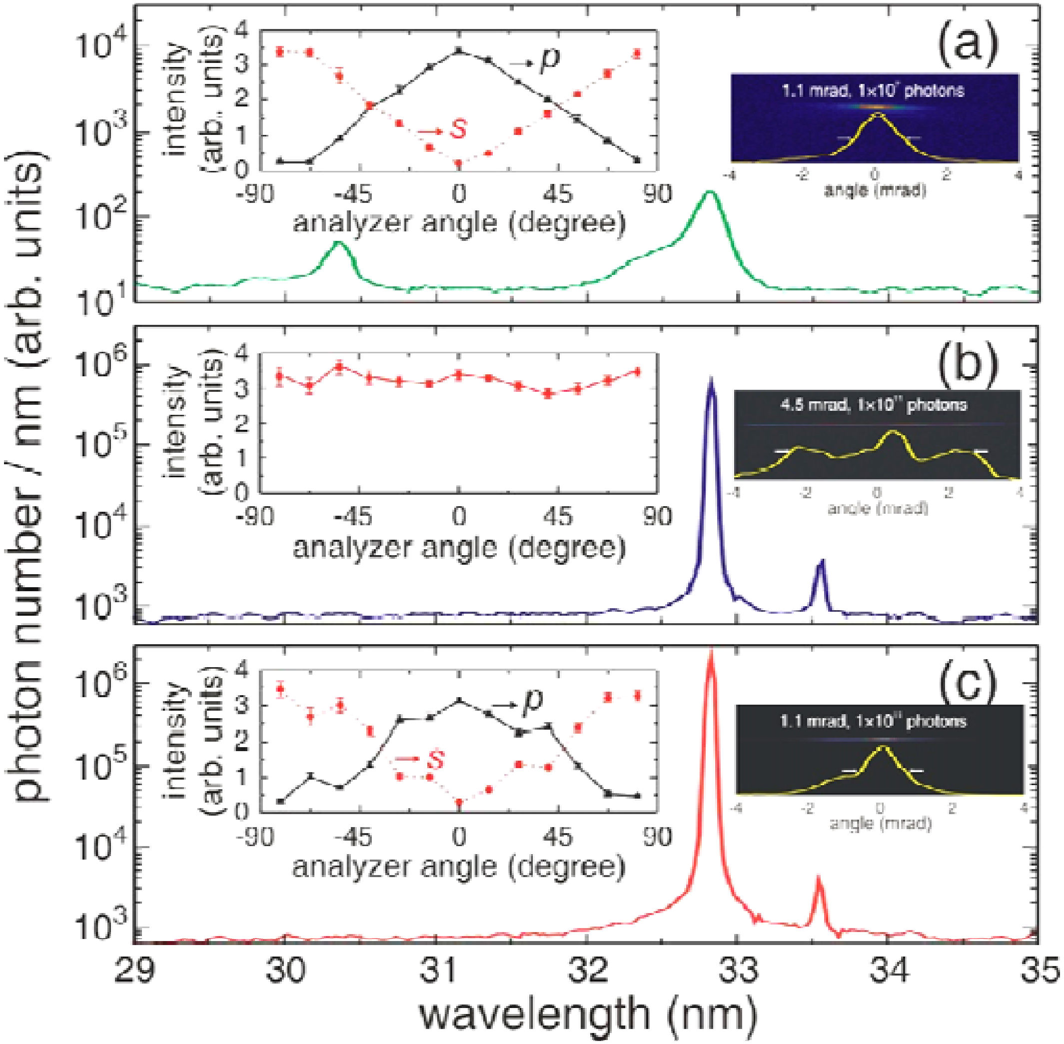

(a) HHG = 10^7 photons/pulse;
1.1 mrad

(b) XRL_{ASE} = 10^{11} photons/pulse
4.5 mrad

(c) XRL_{seeded} =10^{11} photons/pulse
1.1 mrad

Brightness of seeded XRL is
~16X
higher than that of ASE XRL

Peak brilliance and peak power of several existing or planned FEL facilities

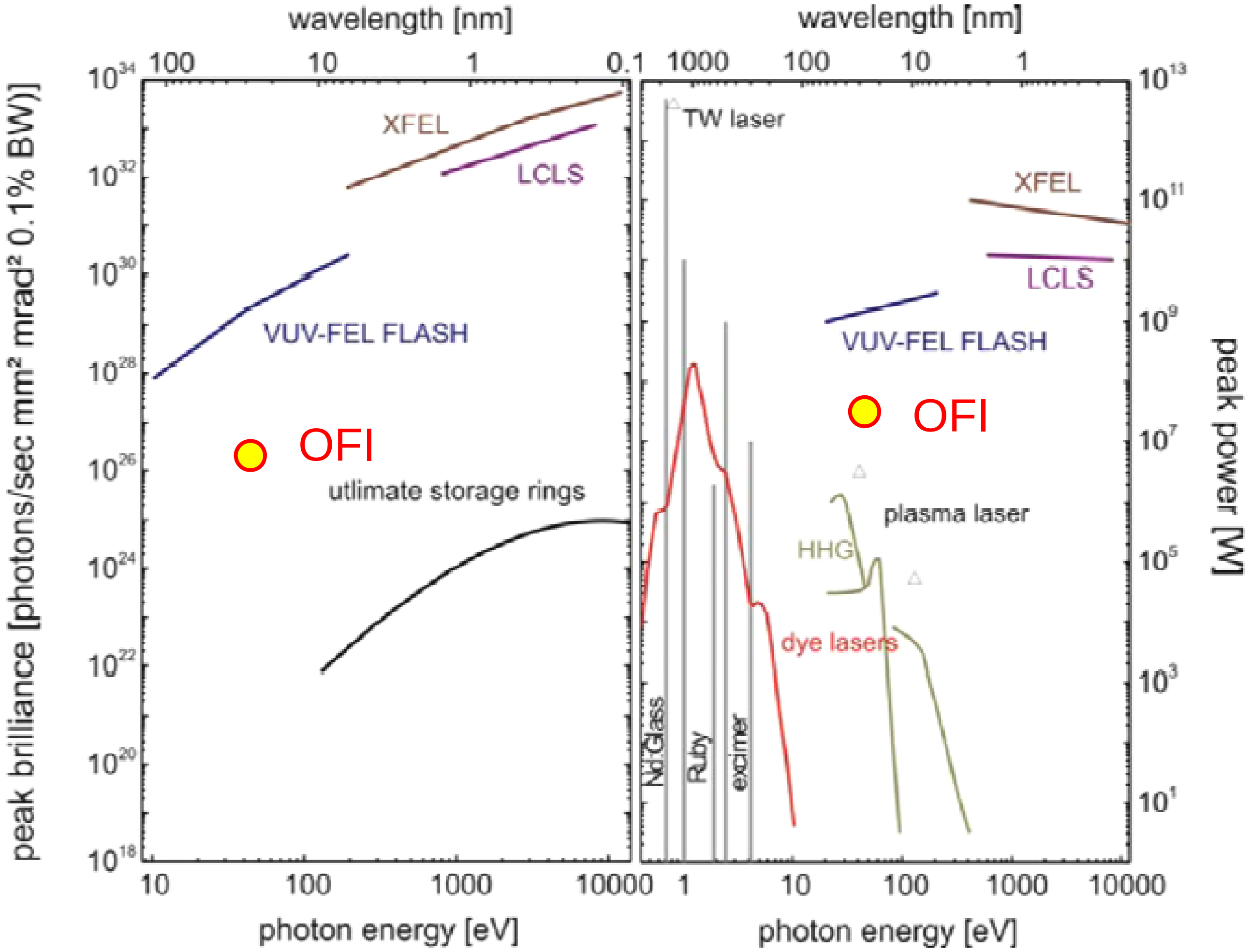

Summary

I. Generations of plasma waveguide channel for OFI X-ray laser generations are achieved. Significant enhancement of output energy of Ni-like Kr laser at 32.8 nm by a factor of >1000 is achieved with respect to that without the plasma waveguide, resulting in a photon number of $\sim10^{12}$.

II. The same method is used to achieve X-ray lasing for the high-threshold low-gain transition at 46.9 nm in Ne-like Ar.

III. Simultaneous lasing of Ar8+ at 46.9 nm and Kr8+ at 32.8 nm is also achieved by using a plasma waveguide of Ar/Kr mixture.

IV. Strongly saturated waveguide-based optical-field-ionization soft-x-ray laser seeded by high harmonic generation is demonstrated for Ni-like Kr lasing at 32.8 nm, yielding much smaller divergence, enhanced spatial coherence, and controlled polarization.

Applications with X-ray lasers

Applications with x-rays

- Science
  - Atomic Physics: photoexcitation, (multiple) photoionization etc.
  - Electron Spectroscopy for Chemical Analysis (ESCA)
  - Diagnostics of High-Density Fusion Plasma
- Technical
  - Grating and Grid Production with X-ray Lasers
  - Photolithography with X-ray lasers
- Biology
  - X-ray Microscopy
  - X-ray Holography
  - X-ray Diffractometry

coherent x-ray imaging

X-ray phase contrast microscopy

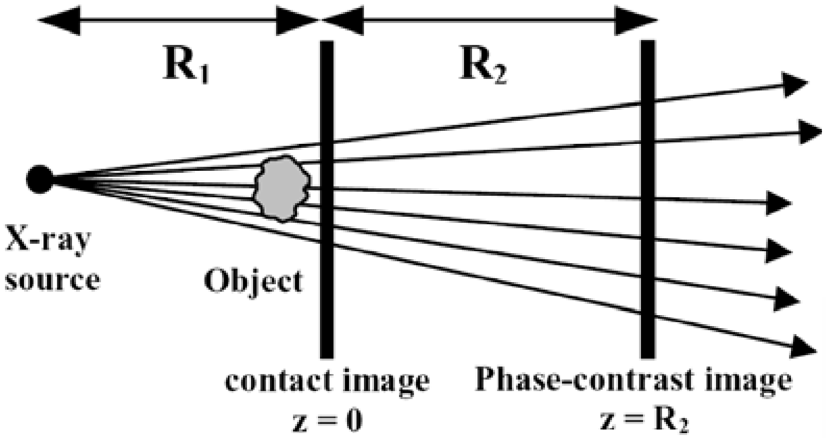

Fresnel diffraction

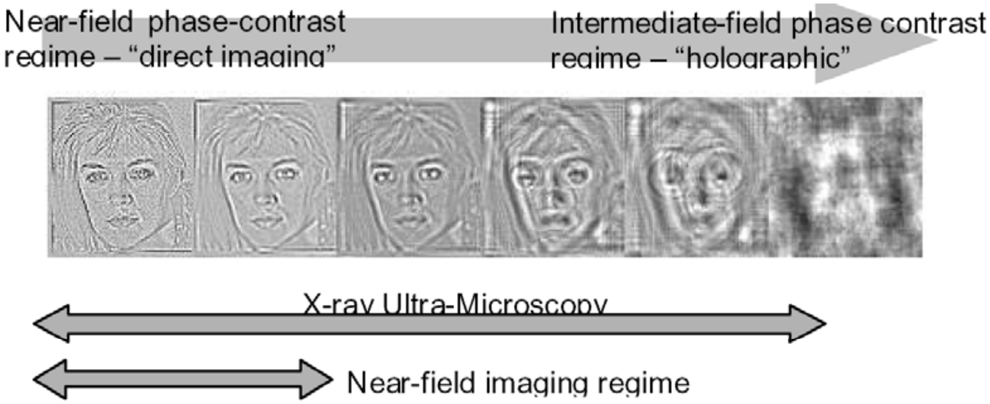

Near-field phase-contrast regime – “direct imaging”

Intermediate-field phase contrast regime – “holographic”

X-ray Ultra-Microscopy

Near-field imaging regime

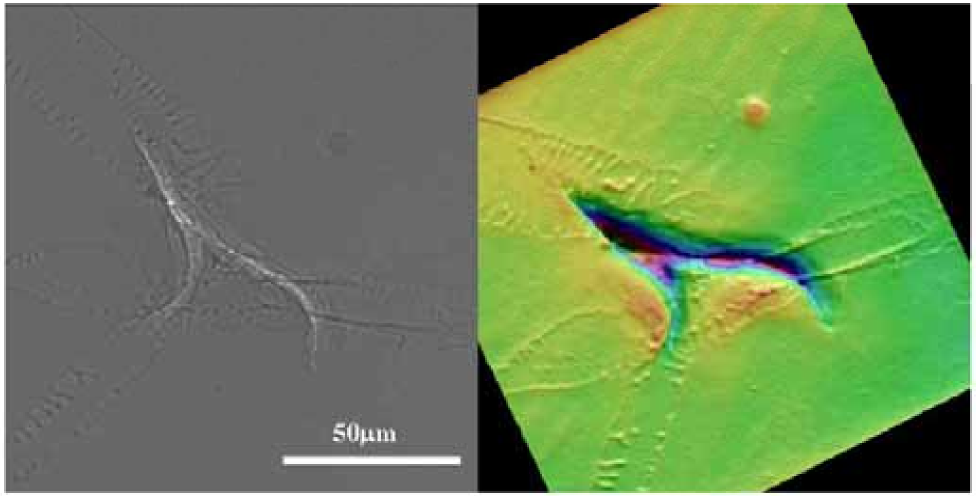

Fig. 6. Phase contrast image (left) and phase retrieved sample thickness for a puncture in a polymer film, acquired with a Ta target at 15kV, R_1=2.8mm, R_1+R_2=250mm, 10 min exposure.

X-ray phase contrast microscopy

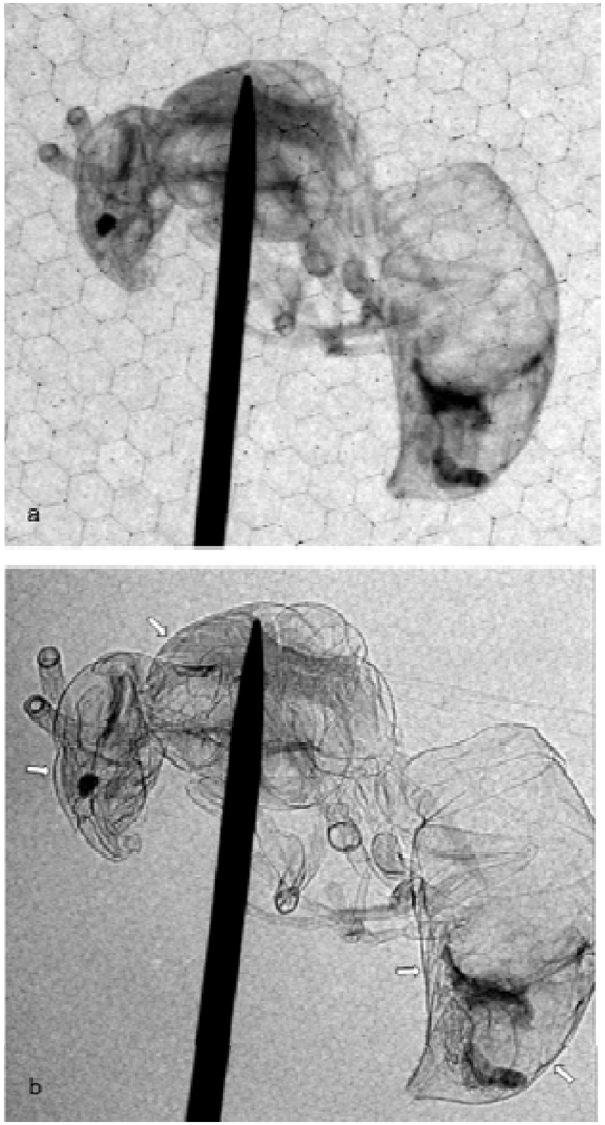

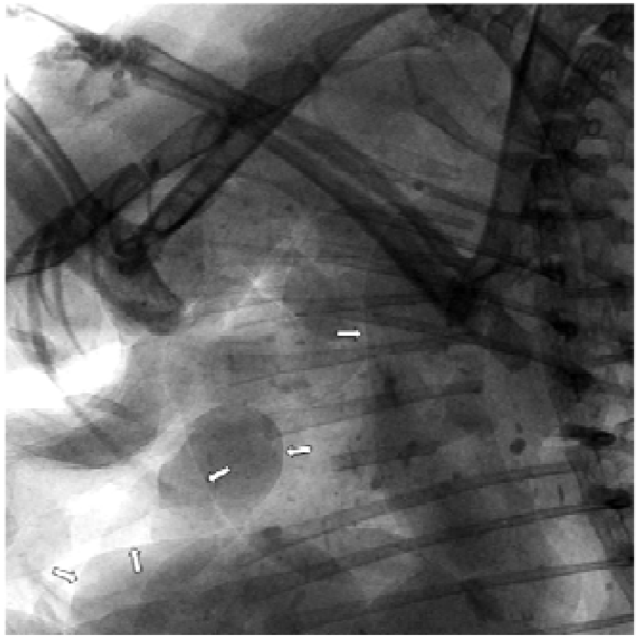

FIG. 7. *In vitro* raw phase-contrast projection image of the abdomen of a 16-week-old mouse (26 g) obtained for ODD=90 cm, SOD=45 cm, and with 17-keV photon fluence on the sample of 3×10^8 photons/cm^2. The arrows indicate internal features enhanced by phase-contrast imaging.

Rev. Sci. Instrum. **76**, 083701 (2005)

X-ray microscopy

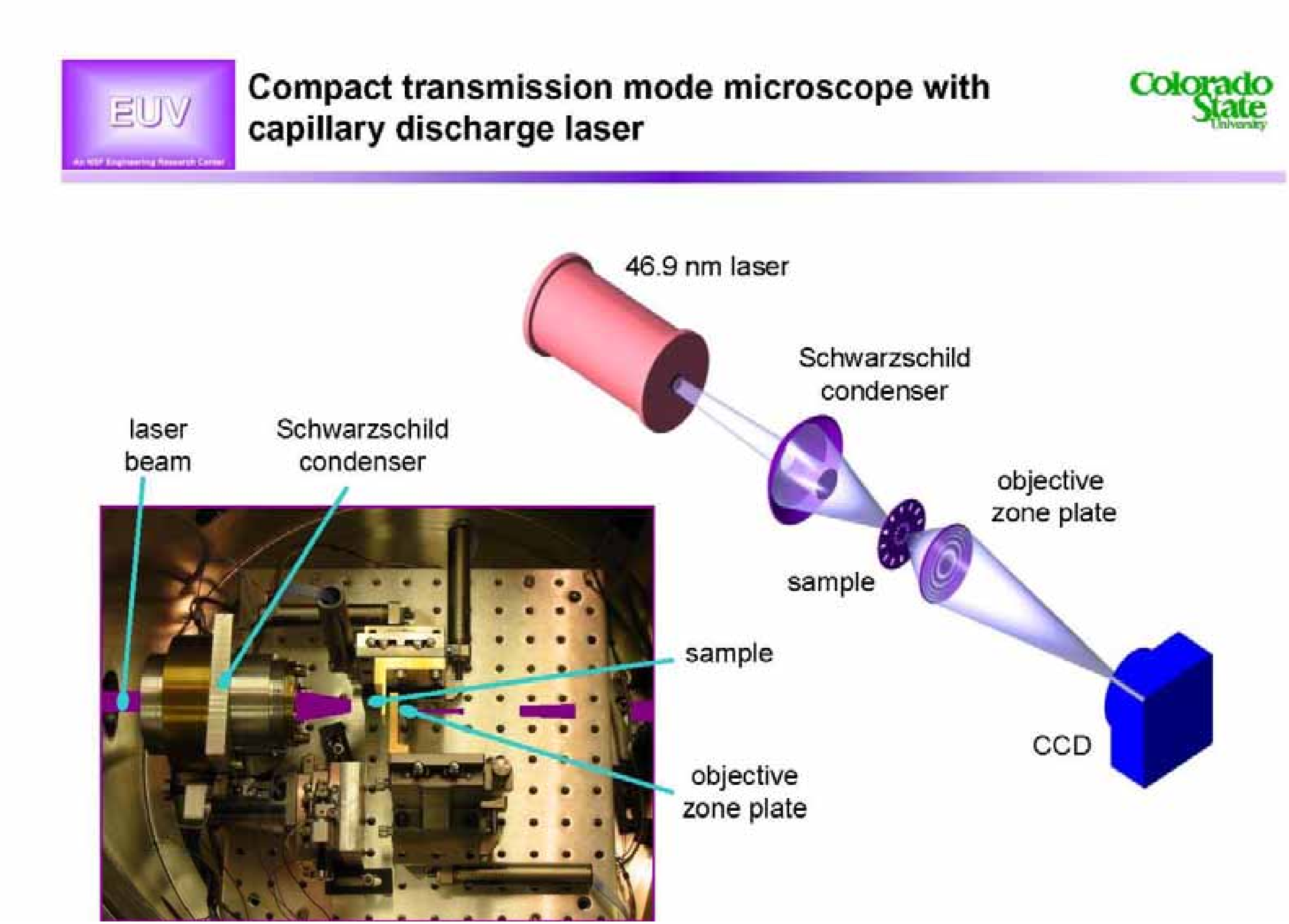

Compact transmission mode microscope with capillary discharge laser

X-ray microscopy

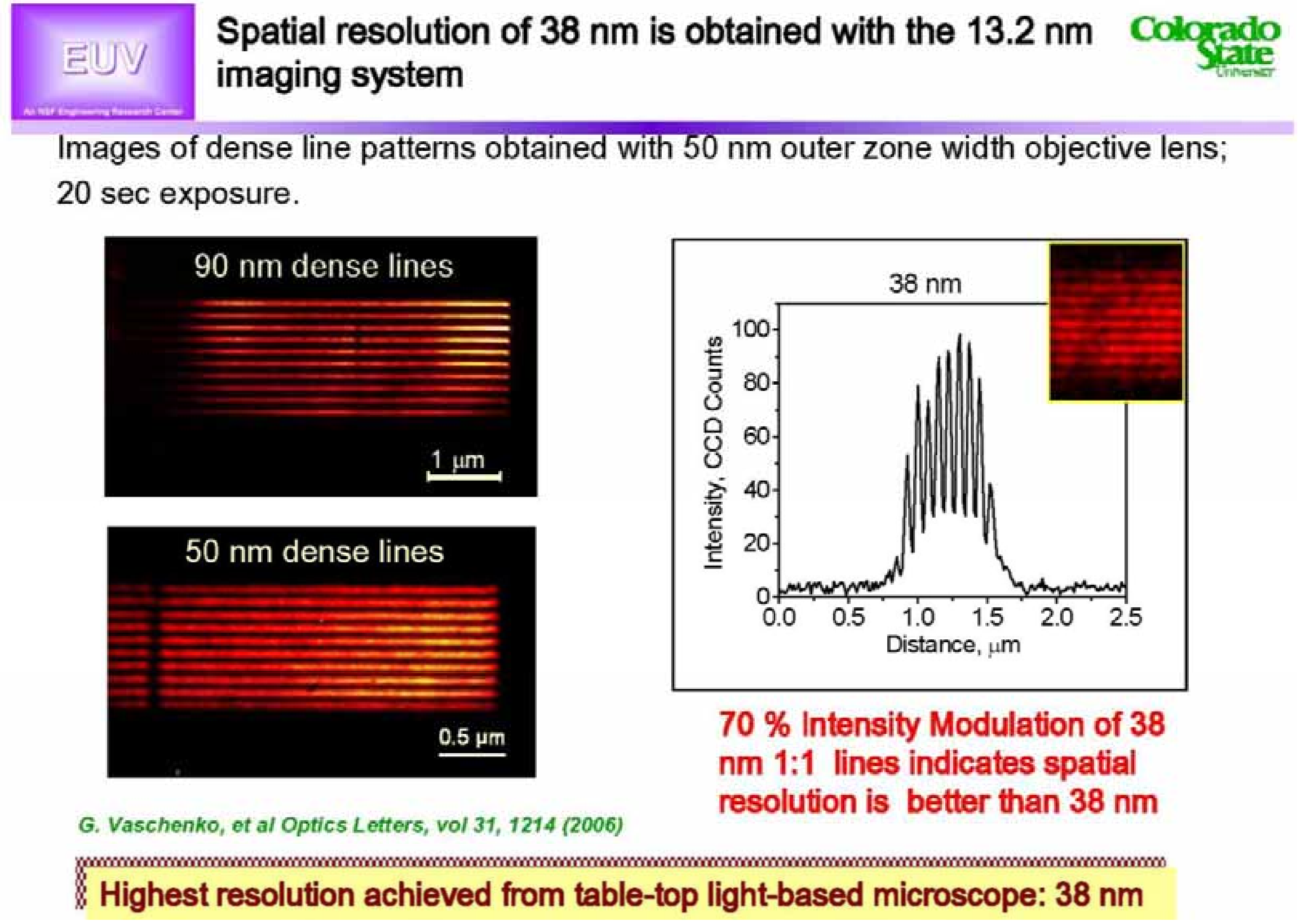

Spatial resolution of 38 nm is obtained with the 13.2 nm imaging system

Images of dense line patterns obtained with 50 nm outer zone width objective lens; 20 sec exposure.

70 % Intensity Modulation of 38 nm 1:1 lines indicates spatial resolution is better than 38 nm

G. Vaschenko, et al Optics Letters, vol 31, 1214 (2006)

Highest resolution achieved from table-top light-based microscope: 38 nm

X-ray digital holographic microscopy

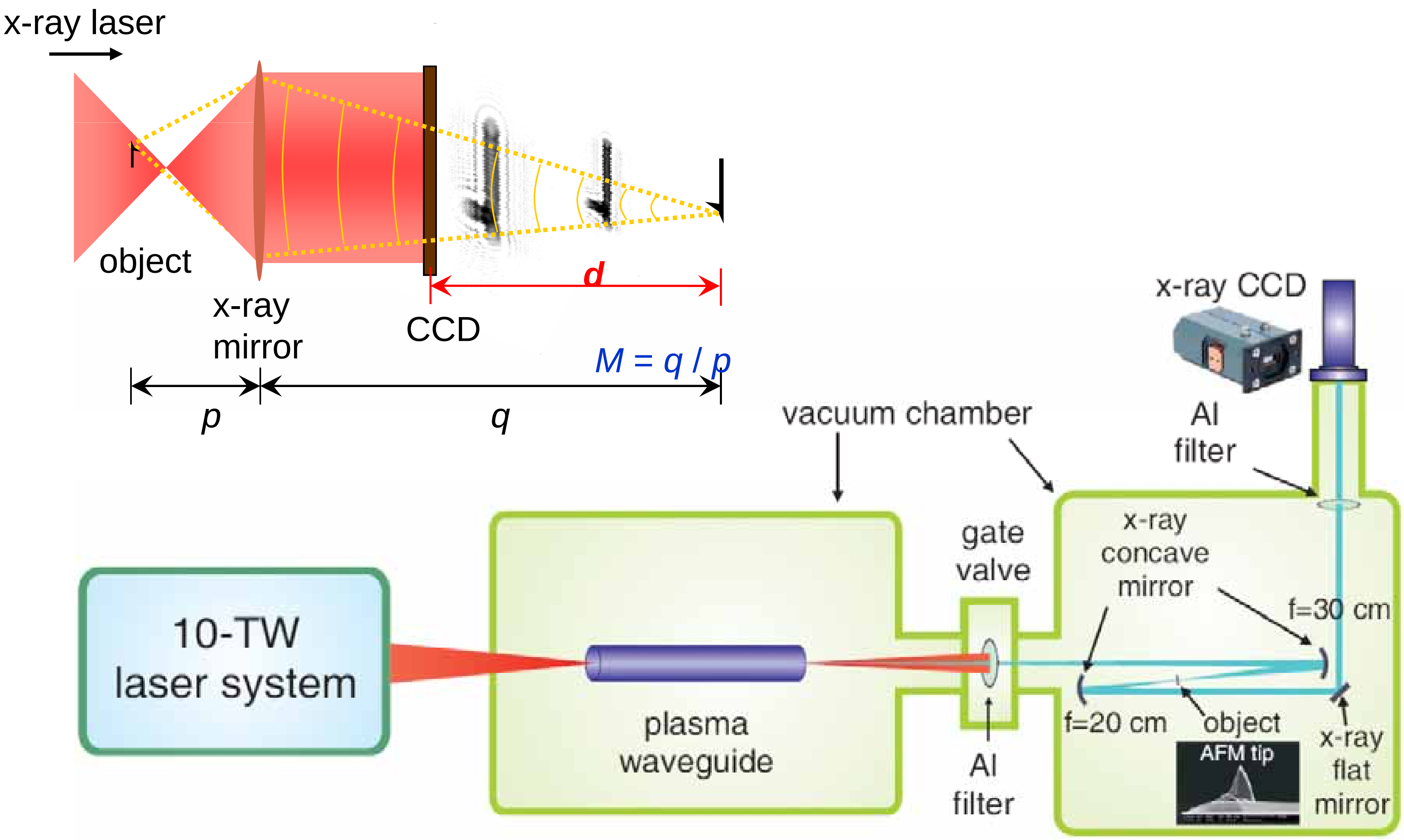

Soft X-ray hologram and reconstructed image of AFM tip with various magnifications

magnification: 11.8X 21.1X 29.7X 46.4X

hologram

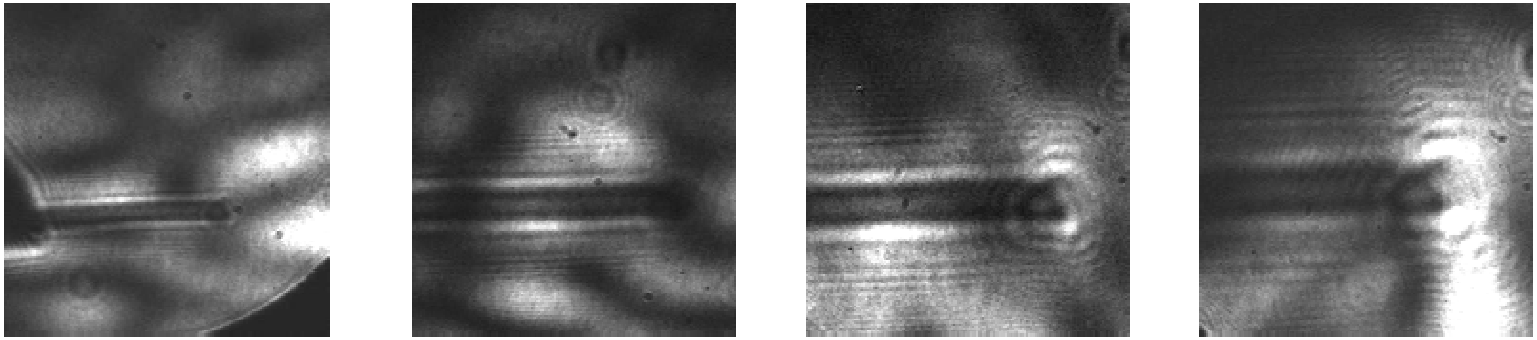

reconstructed image

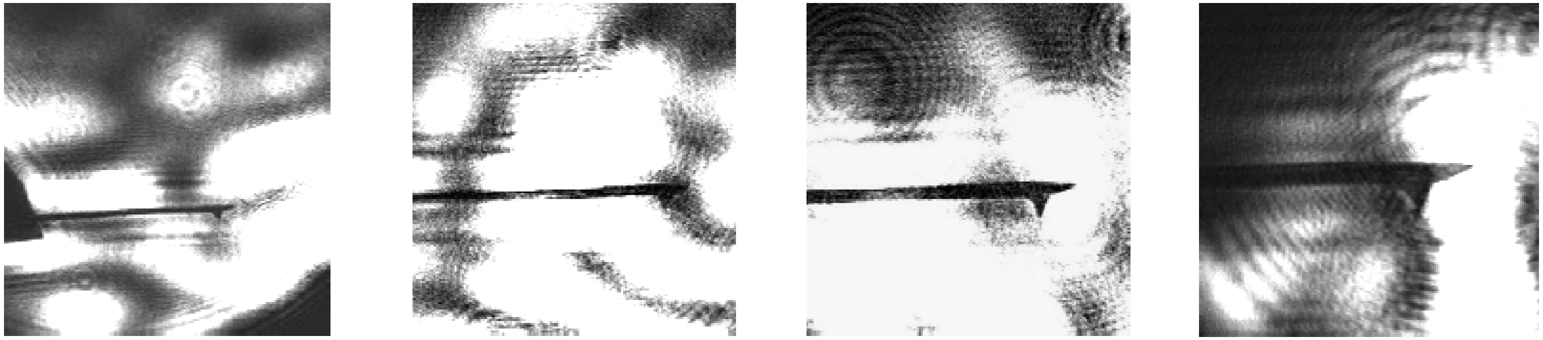

Carbon foil images with various magnifications

magnification:	15.8X	17.9X	28.7X	54.4X
distance to mirror	@25.53 cm	@25.34 cm	@24.84 cm	@24.44 cm

6.2X
@27.85 cm

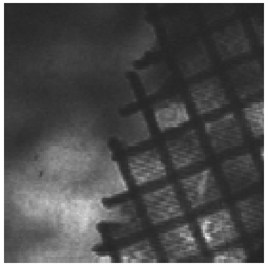

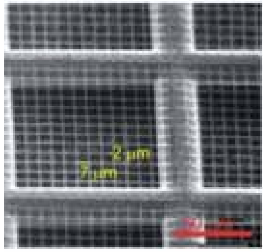

hologram

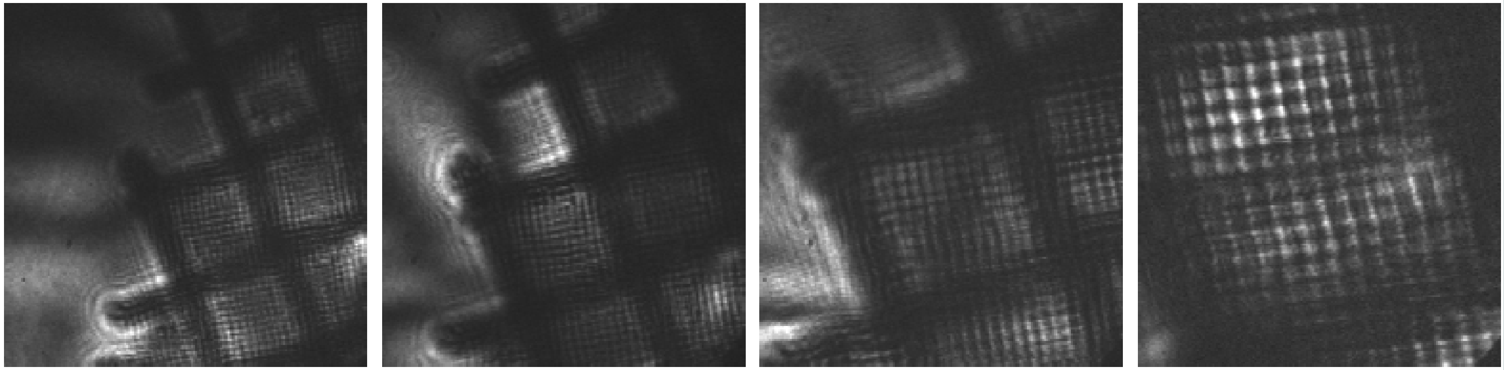

reconstructed image

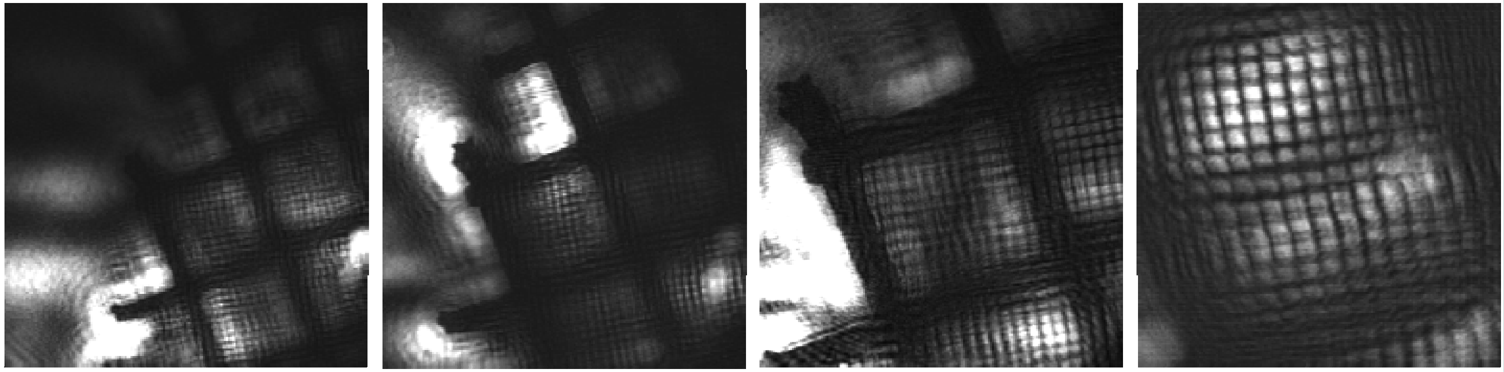

Amplitude and phase reconstruction for carbon foil

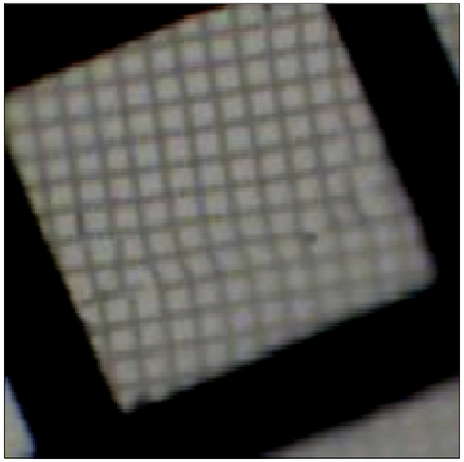

by optical microscope

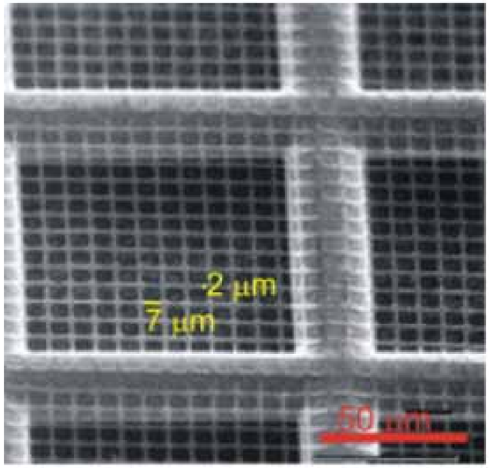

from manufacture data

bar width = 2 μm
thickness = 20 ± 3 nm

reconstructed
amplitude image

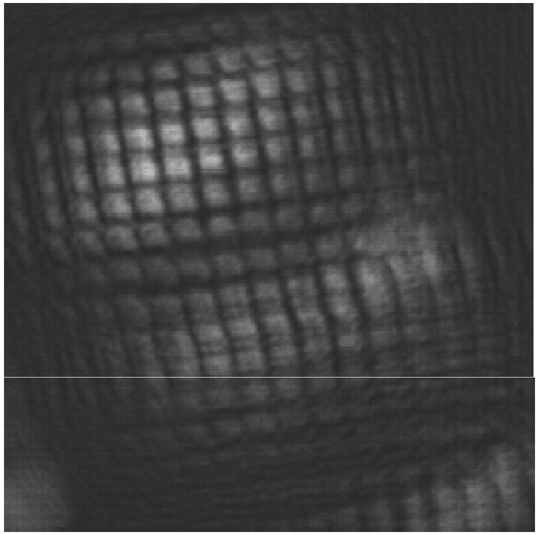

reconstructed
phase image

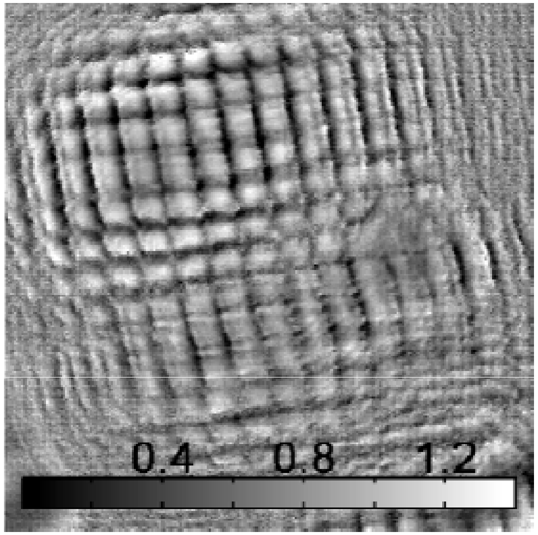

retrieved phase difference
= 0.8 ~ 1.2 rad (19 ~ 28 nm)

X-ray coherent diffraction imaging

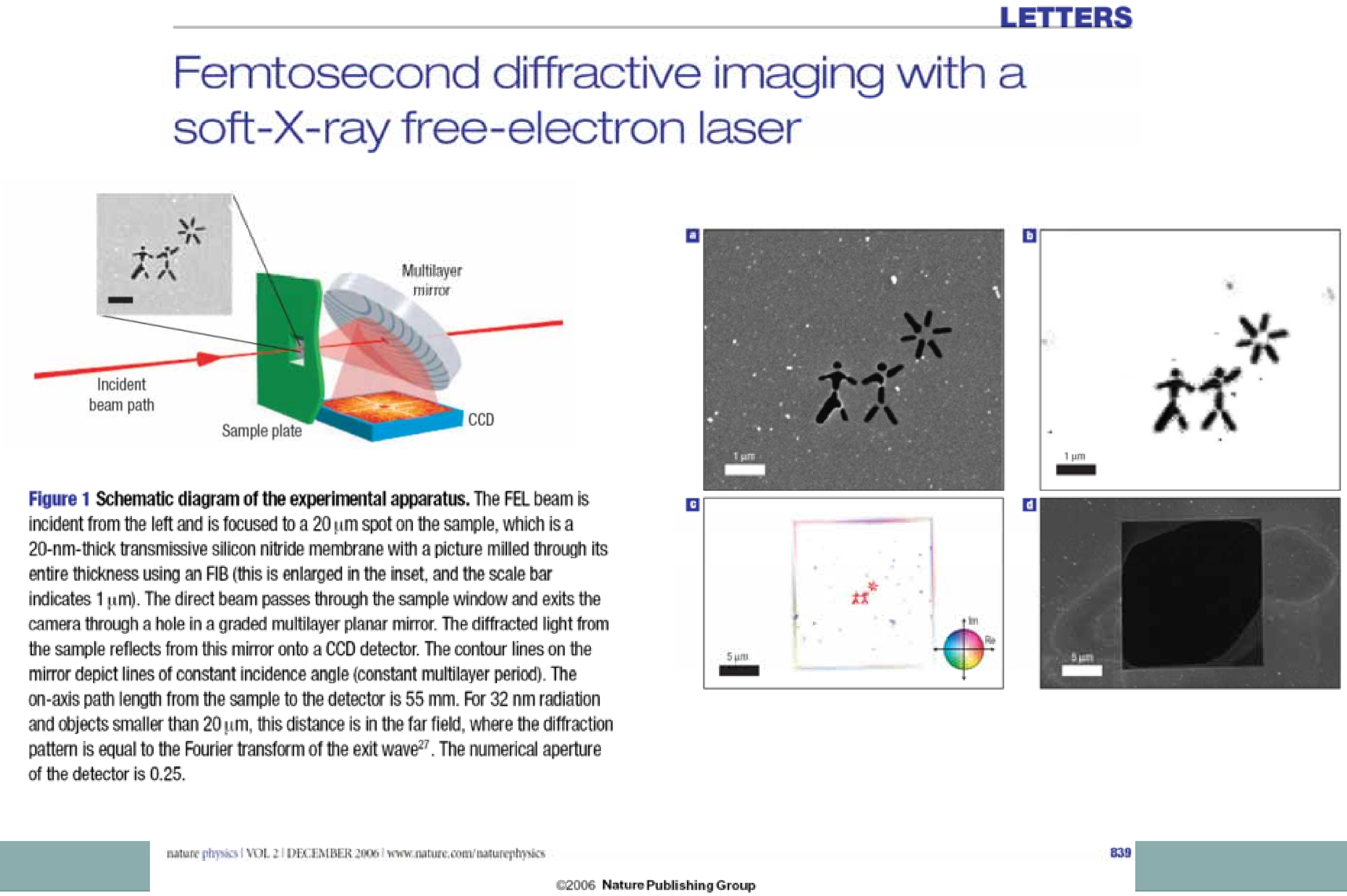

LETTERS

Femtosecond diffractive imaging with a soft-X-ray free-electron laser

Figure 1 **Schematic diagram of the experimental apparatus.** The FEL beam is incident from the left and is focused to a 20 μm spot on the sample, which is a 20-nm-thick transmissive silicon nitride membrane with a picture milled through its entire thickness using an FIB (this is enlarged in the inset, and the scale bar indicates 1 μm). The direct beam passes through the sample window and exits the camera through a hole in a graded multilayer planar mirror. The diffracted light from the sample reflects from this mirror onto a CCD detector. The contour lines on the mirror depict lines of constant incidence angle (constant multilayer period). The on-axis path length from the sample to the detector is 55 mm. For 32 nm radiation and objects smaller than 20 μm, this distance is in the far field, where the diffraction pattern is equal to the Fourier transform of the exit wave[27]. The numerical aperture of the detector is 0.25.

X-ray coherent diffraction imaging

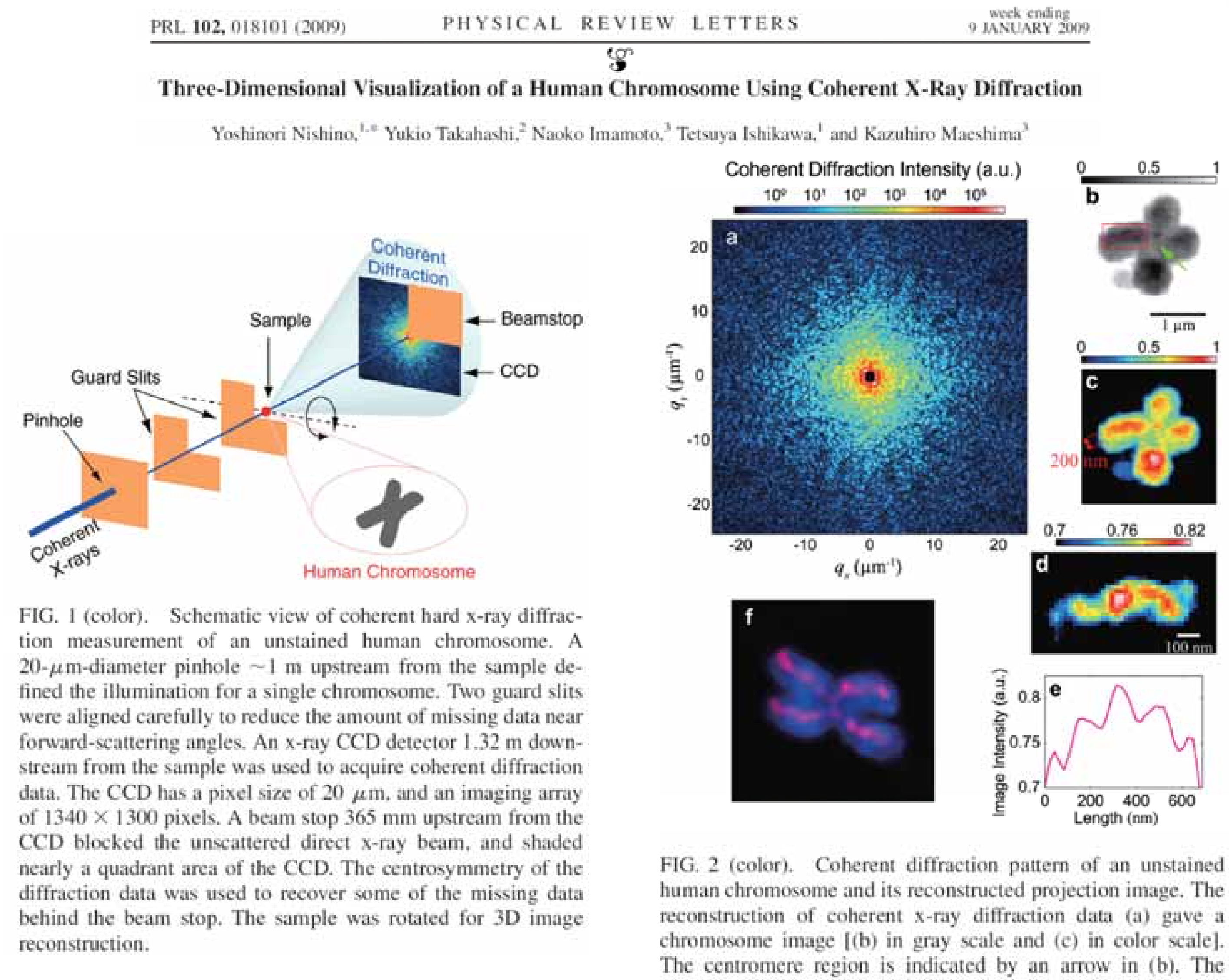

PRL **102,** 018101 (2009) PHYSICAL REVIEW LETTERS week ending 9 JANUARY 2009

Three-Dimensional Visualization of a Human Chromosome Using Coherent X-Ray Diffraction

Yoshinori Nishino,[1,*] Yukio Takahashi,[2] Naoko Imamoto,[3] Tetsuya Ishikawa,[1] and Kazuhiro Maeshima[3]

FIG. 1 (color). Schematic view of coherent hard x-ray diffraction measurement of an unstained human chromosome. A 20-μm-diameter pinhole ~1 m upstream from the sample defined the illumination for a single chromosome. Two guard slits were aligned carefully to reduce the amount of missing data near forward-scattering angles. An x-ray CCD detector 1.32 m downstream from the sample was used to acquire coherent diffraction data. The CCD has a pixel size of 20 μm, and an imaging array of 1340 × 1300 pixels. A beam stop 365 mm upstream from the CCD blocked the unscattered direct x-ray beam, and shaded nearly a quadrant area of the CCD. The centrosymmetry of the diffraction data was used to recover some of the missing data behind the beam stop. The sample was rotated for 3D image reconstruction.

FIG. 2 (color). Coherent diffraction pattern of an unstained human chromosome and its reconstructed projection image. The reconstruction of coherent x-ray diffraction data (a) gave a chromosome image [(b) in gray scale and (c) in color scale]. The centromere region is indicated by an arrow in (b). The

Long exposure time !!

X-ray flash imaging

Potential for biomolecular imaging with femtosecond X-ray pulses

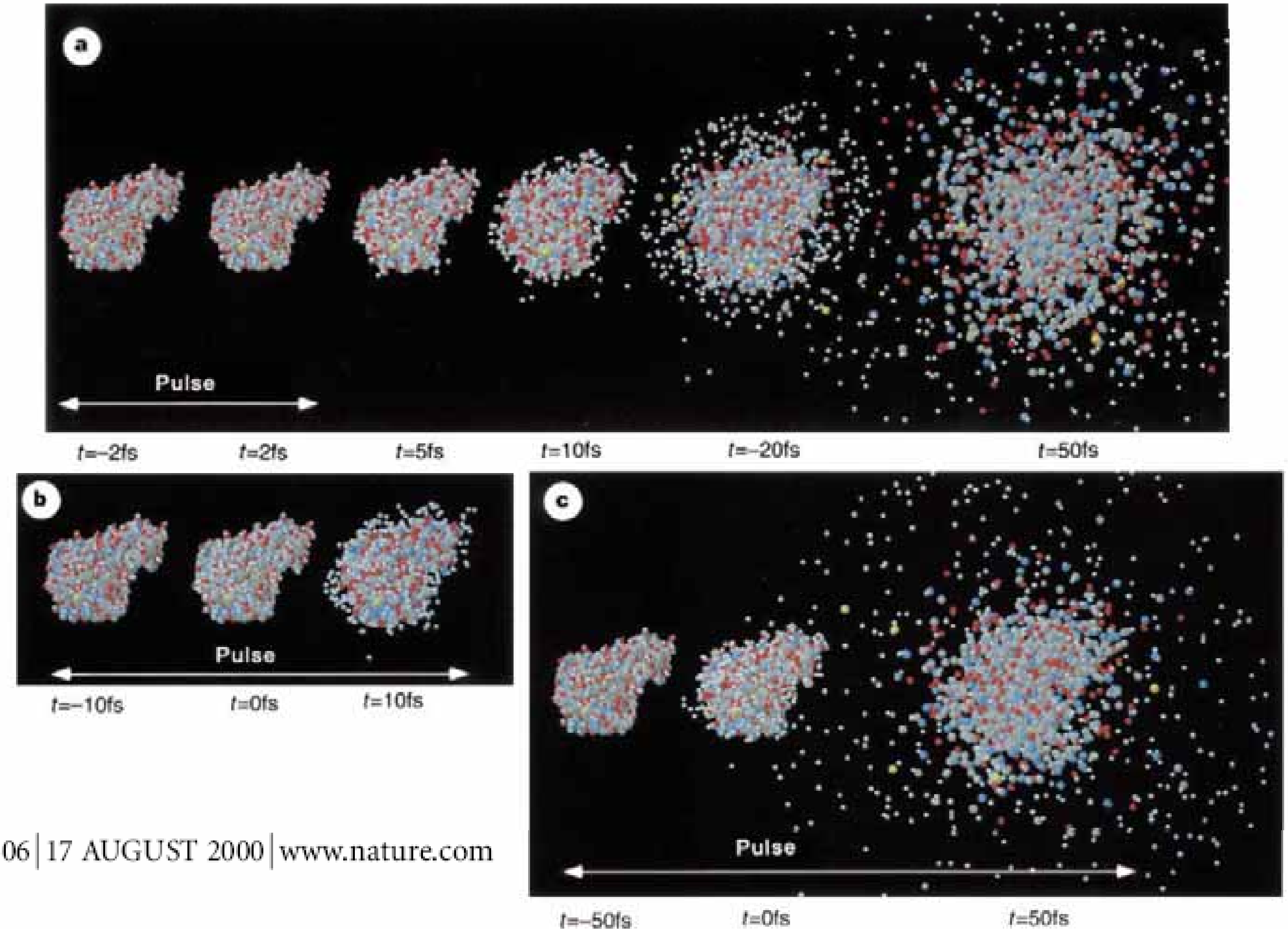

NATURE | VOL 406 | 17 AUGUST 2000 | www.nature.com

Attosecond science

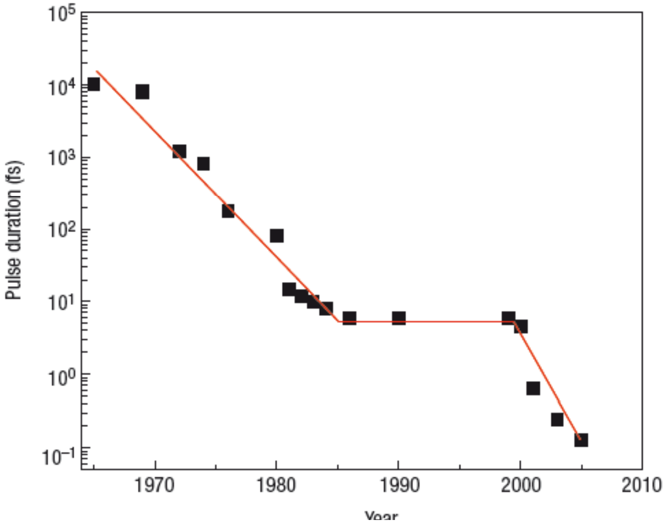

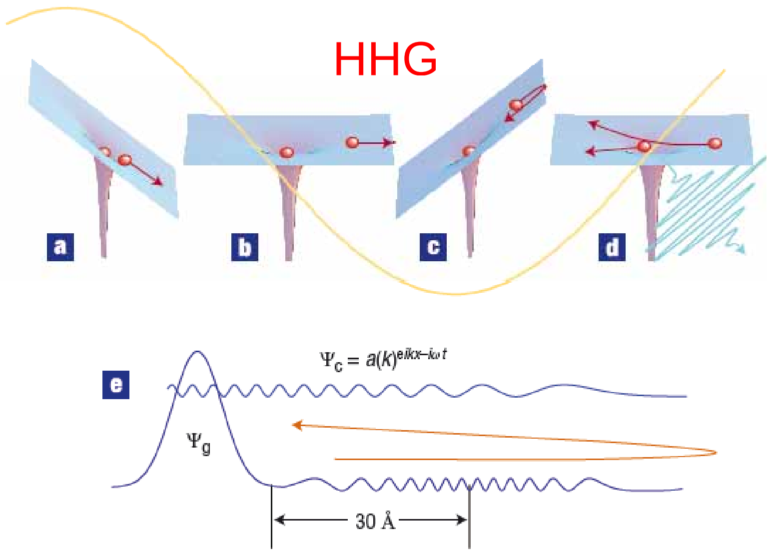

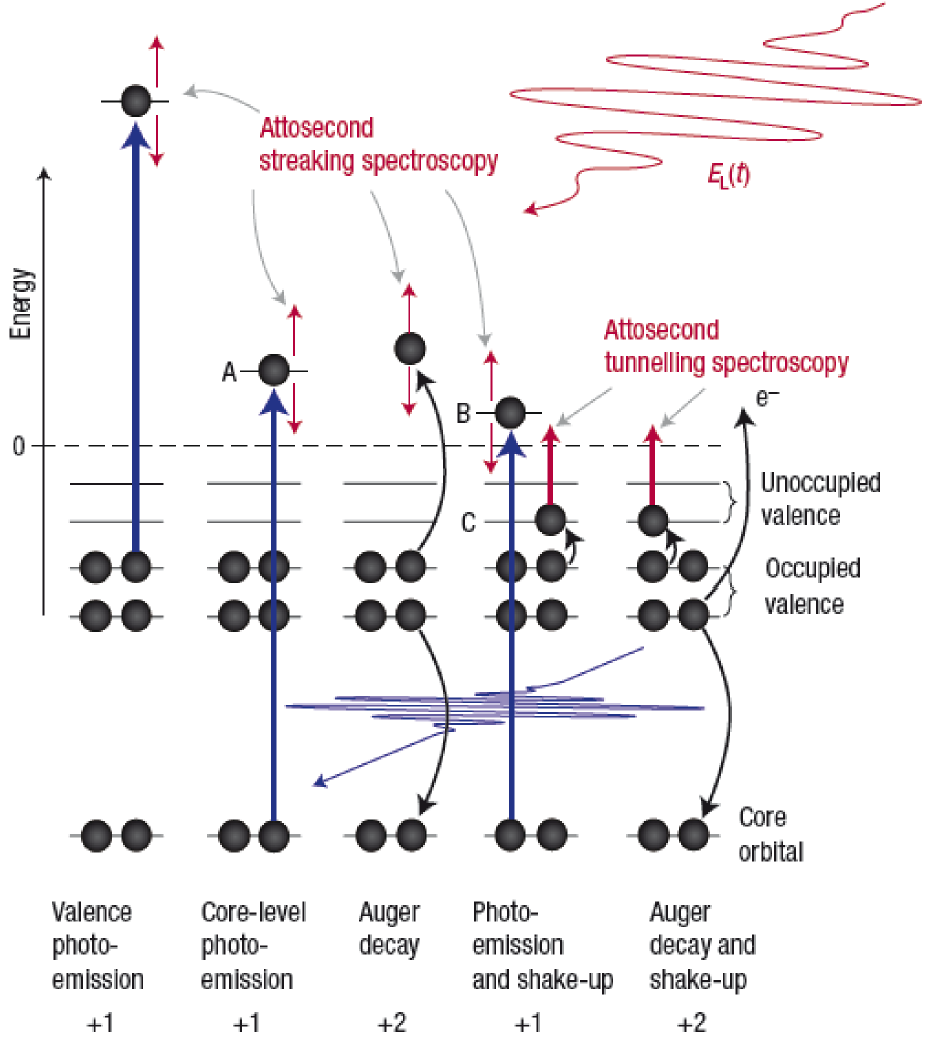

EUV lithography with 13.5 nm light source

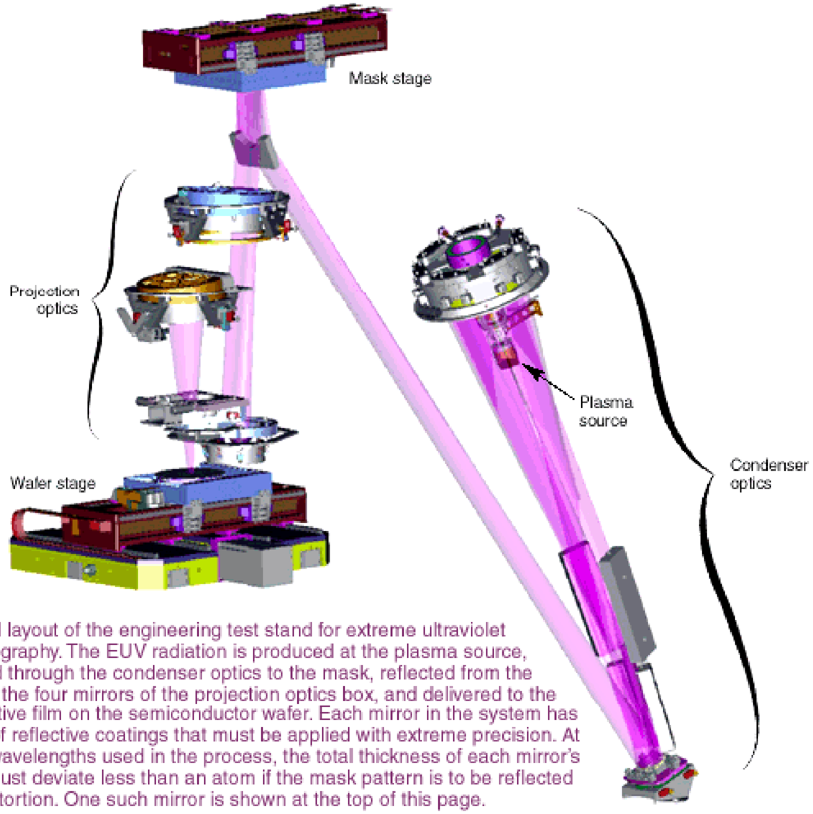

The optical layout of the engineering test stand for extreme ultraviolet (EUV) lithography. The EUV radiation is produced at the plasma source, transmitted through the condenser optics to the mask, reflected from the mask onto the four mirrors of the projection optics box, and delivered to the EUV-sensitive film on the semiconductor wafer. Each mirror in the system has 81 layers of reflective coatings that must be applied with extreme precision. At the short wavelengths used in the process, the total thickness of each mirror's coatings must deviate less than an atom if the mask pattern is to be reflected without distortion. One such mirror is shown at the top of this page.

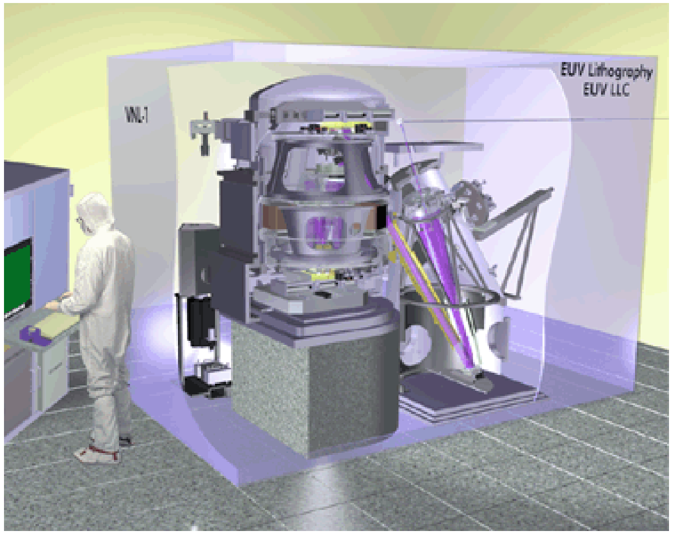

A conceptual drawing of the extreme ultraviolet engineering test stand. The goal of the ETS is to demonstrate how ultraviolet wavelengths can be used to print patterns on integrated circuits at production levels and sizes.

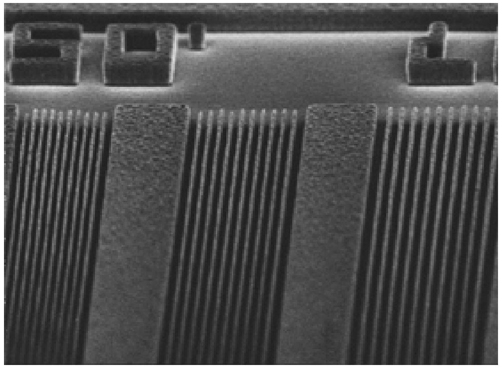

Using a prototype system, the Virtual National Laboratory has successfully printed lines as small as 50 nanometers (billionths of a meter) wide in photoresist. Current lithographic tools used in the semiconductor industry print patterns with 180-nanometer-size features.

High-intensity transient plasma photonic devices with spatio-temporal pulse-shaping

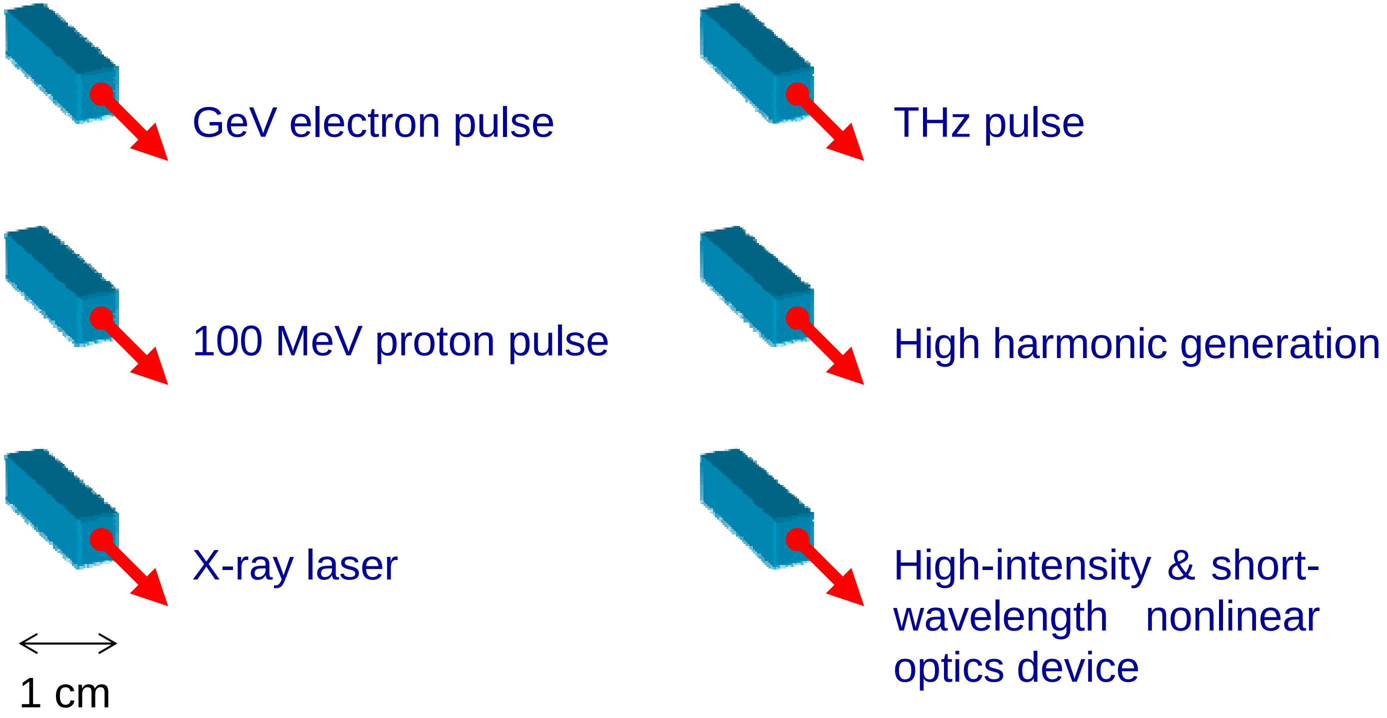

GeV electron pulse

THz pulse

100 MeV proton pulse

High harmonic generation

X-ray laser

High-intensity & short-wavelength nonlinear optics device

Thanks for your attention!